Natural Resources Canada | Ressources naturelles Canada

GEOLOGICAL SURVEY OF CANADA
OPEN FILE 8905

3D regional-scale modelling of the Flin Flon – Glennie complex: preparatory data analysis and preliminary results, Manitoba and Saskatchewan

E.M. Schetselaar, D. White, O. Boulanger, J.A. Craven, G. Bellefleur, and S.M. Ansari

2022

Canada

ISSN 2816-7155
ISBN 978-0-660-44276-1
Catalogue No. M183-2/8905E-PDF

GEOLOGICAL SURVEY OF CANADA
OPEN FILE 8905

3D regional-scale modelling of the Flin Flon – Glennie complex: preparatory data analysis and preliminary results, Manitoba and Saskatchewan

E.M. Schetselaar, D. White, O. Boulanger, J.A. Craven, G. Bellefleur, and S.M. Ansari

2022

Permanent link : https://doi.org/10.4095/330304

This publication is available for free download through GEOSCAN (https://geoscan.nrcan.gc.ca/).

Recommended citation
Schetselaar, E.M., White, D., Boulanger, O., Craven, J.A., Bellefleur, G., and Ansari, S.M., 2022. 3D regional-scale modelling of the Flin Flon – Glennie complex: preparatory data analysis and preliminary results, Manitoba and Saskatchewan; Geological Survey of Canada, Open File 8905, 33 p. https://doi.org/10.4095/330304

Publications in this series have not been edited; they are released as submitted by the author.

TABLE OF CONTENTS

LIST OF FIGURES

LIST OF TABLES

SUMMARY

This Open File reports progress of a 3D regional-scale modelling research project undertaken in the Flin Flon – Glennie Complex of Manitoba and Saskatchewan. The principle focus of this project is to advance methods for deep exploration by developing integrated 3D modelling approaches that employ multi-parameter geophysical surveys and subsurface geological data. This report summarizes method development, preparatory data analysis and preliminary interpretations of individual data components, including 3D inverse models of regional potential field and LITHOPROBE magnetotelluric data, inverse electromagnetic (EM) modelling method development with results from the Lalor camp, a status report for the acquisition of a new high-resolution Denare Beach seismic profile, a harmonized drillhole-bedrock compilation of the Flin Flon mining district and a preliminary crustal model of the Western Flin Flon – Glennie Complex.

INTRODUCTION

In 2018, the Geological Survey of Canada (GSC) initiated a research project to develop methods for constructing a regional-scale 3D model of the Flin Flon – Glennie Complex (FFGC) to enhance the effectiveness of deep mineral exploration. The over-arching objective is to develop and test novel methods for integrated regional-scale 3D modelling that will ultimately allow building of the first 3D greenstone belt model in Canada. This regional-scale 3D modelling initiative started out as a two-year pilot project funded by the National Geological Survey Committee of Canada (NGSC) as part of a collaboration with the Saskatchewan and Manitoba geological surveys. In the second half of 2020, the project received additional funds from the 6th Phase of the Targeted Initiative Program, which allowed the acquisition of a high-resolution seismic profile between Flin Flon and Amisk Lake.

Scope

3D geological models provide knowledge of the subsurface geology that is essential for deep exploration. Insight into the 3D geological structure of the subsurface not only allows outlining the subsurface extent of mineral deposits already discovered, but also aids geophysical exploration in the prediction of favourable settings for new discoveries. Hence, 3D geological modelling provides excellent value in any exploration campaign, particularly when it informs drill targeting. On the other hand, in complex geological settings, such as the Canadian Shield, 3D geological models not only guide drilling but, conversely, heavily depend on drillhole availability: drillhole markers of geological unit contacts and structures are the sole source of *in situ* information supplying subsurface constraints for 3D geological modelling. This explains why in complex hard rock settings, such as the Canadian Shield, 3D geological models are usually only available at mine-camp scale. Upscaling 3D geological models from these so-called '*brownfield*' settings to regional scale '*greenfield'* domains would be a substantial breakthrough in guiding deep exploration, which, due to the sparse and clustered distribution of drillholes is a significant challenge. Confronting this challenge, requires an integrated forward and inverse modelling approach, which reconciles geophysical models with respect to each other, with respect to geological data (e.g., drillholes and geological maps) and with respect to physical rock properties (e.g., density, magnetic susceptibility, electric conductivity, seismic velocity). The aim of this project is to develop such an integrated modelling approach and test the methods and

algorithms that formally integrate the various components of information from mining camp to lithospheric scales to facilitate scenario-testing and/or probabilistic assessment of the results.

The Flin Flon Glennie Complex testbed

The 3D modelling methodology will be applied using geophysical and geological exploration data acquired in the FFGC of Manitoba and Saskatchewan, Canada. This greenstone belt is, for several reasons, considered an ideal test bed for addressing the integrated 3D modelling approach:

1. It is one of the most prolific greenstone belts in Canada, well known for its numerous volcanogenic massive sulfide (VMS) and precious metal deposits.
2. It provides a rich 2D and 3D geological database, including bedrock maps, geological compilations of prospective bedrock geology under Phanerozoic cover, camp-scale 3D geological models and industry drillhole data, accessible via data sharing agreements.
3. The belt is covered by multi-parameter geophysical surveys, including LITHOPROBE seismic and MT regional profiles, medium-resolution potential field surveys, high-resolution seismic profiles and seismic cubes in mining districts and multi-parameter airborne and ground-based (downhole) EM surveys.
4. Legacy crustal-scale 3D regional models of the FFGC are available. Although these models are mainly schematic, being compiled from regional seismic interpretation and geological map compilations, they provide a convenient baseline for the data-constrained 3D modelling objectives of this project.
5. As the FFGC comprises exposed and covered parts, both with favourable geology for base metal and gold deposits, it allows testing under cover exploration scenarios, using the better-known exposed part of the belt for calibration purposes.

The main deliverable of this multidisciplinary research project will be a regional 3D knowledge cube of the FFGC that hosts several highly detailed 3D models in chosen sub-regions. This knowledge cube will be accessible on the internet in support of follow-up crustal-scale geological studies and deep exploration targeting. The purpose of this report is to report progress by summarizing the preparatory studies thus far conducted for the project. Figure 1 shows the areas and profiles covered by these studies together with the recently acquired airborne geophysical surveys.

Regional geological setting

The FFGC is a tectonic collage of accreted 1.92–1.88 Ga juvenile arc and oceanic floor terranes (Stern et al. 1995; Syme et al. 1999) in the internal zone of the Trans-Hudson Orogen (THO) intruded by 1.87–1.84 Ga successor arc plutons and overlain by marine and continental 1.85–1.83 Ga clastic sedimentary rocks of the Burntwood and Missi Groups (Lucas et al., 1996, Fig. 2). The exposed portion of the FFGC extends for about 250 km in the east-west direction and 40 km in the north-south direction from its gradual contact with high-grade metamorphic rocks of the Kisseynew domain in the north to its unconformable contact with Phanerozoic cover in the south (Fig. 2). The largest part of the belt, however, extends under Phanerozoic cover that gradually increases in thickness towards the south. The FFGC evolved in four stages, including: (1) formation of a series of juvenile arcs, back-arc basins and ocean plateaus (2) intra-oceanic accretion

followed by (3) successor arc magmatism and development of flysch and molasse basins as a result of ocean closure and convergence of the Archean Hearne, Superior and Sask cratons and (4) further imbrication of the juvenile arc and ocean floor terranes with the younger successor arc magmatic and sedimentary rocks during collisional stages of the Trans Hudson orogeny (Lucas et al., 1996; Corrigan et al., 2009 and references therein). The first-order principal structures of the FFGC comprise a series of arcuate ductile, brittle-ductile shear zones and faults that accommodated intra-oceanic, post-accretion structural telescoping

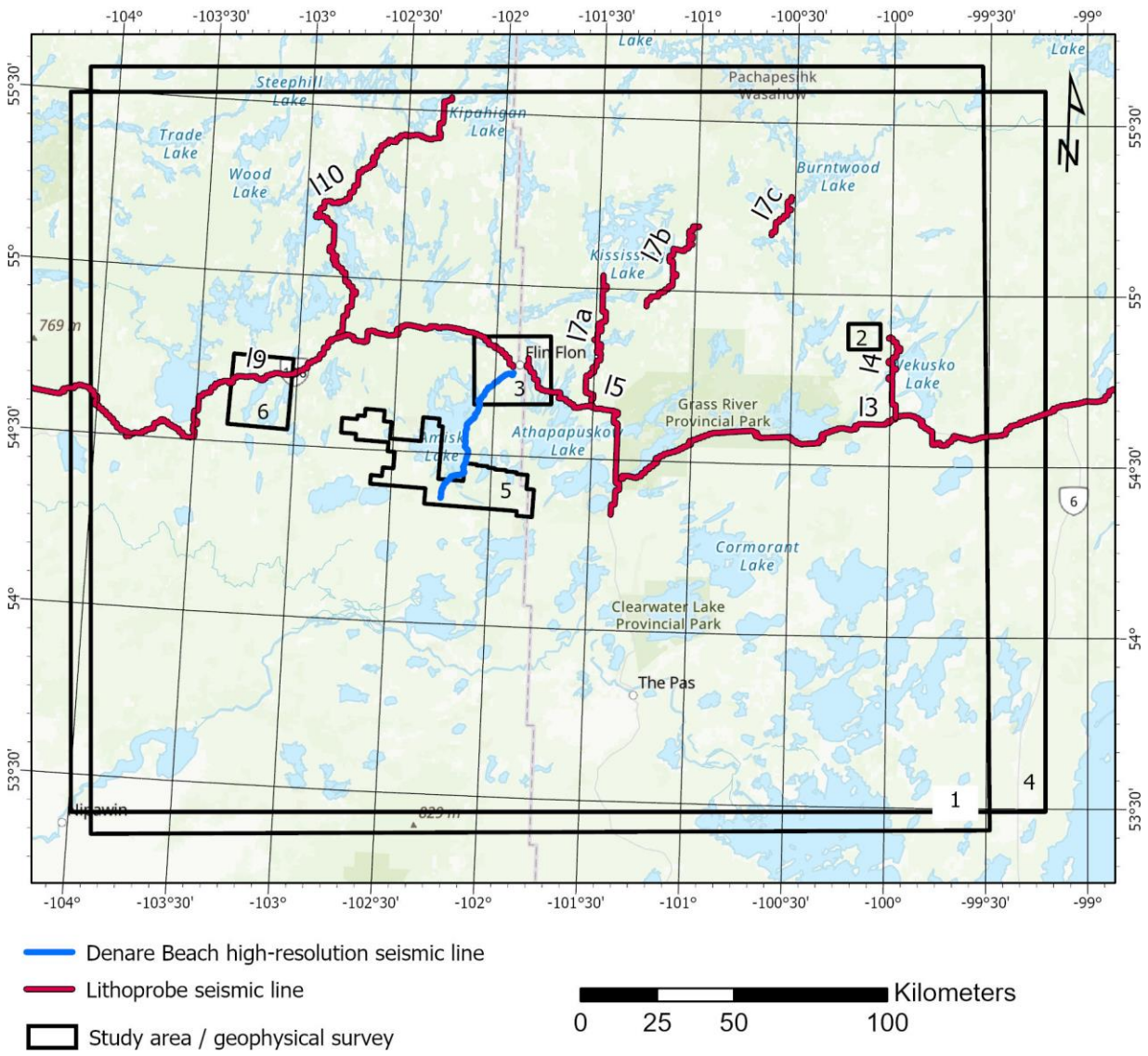

Figure 1 Outlines of study areas and geophysical surveys reported on in this GSC Open File: 1 = regional potential field inversion, 2 = Lalor MT inversion, 3 = harmonized drillhole-bedrock compilation, 4 = preliminary crustal model, 5 = airborne gravity survey, 6 = airborne EM survey. The regional MT inversion was conducted along LITHOPROBE lines 3, 5 and 9.

and strike-slip movements, forming a tectonic collage of 1.88–1.92 Ga pre-accretion, dominantly mafic, metavolcanic assemblages, 1.84–1.83 Ga felsic to mafic plutonic rocks and 1.85–1.83 Ga turbiditic and molasse-like clastic metasedimentary assemblages (Lucas et al. 1996; Stern et al. 2000, Fig. 2). Contrary to the correlation of these metasedimentary rocks (the Burntwood and Missi Groups across the FFGC and their high-grade metamorphic equivalents in the Kisseynew domain, Fig. 2) there is no evident regional correlation between the 1.92–1.88 Ga juvenile arc assemblages (Lucas et al., 1999). This lack of stratigraphic correlation may be due to their distinct primary origin (they are the remnants of distinct arcs) or is perhaps only apparent, as rapid lateral variations in volcanic and volcaniclastic lithofacies in rifted juvenile arc settings may render stratigraphic correlation across first-order fault structures unresolvable. The FFGC is one of the most prolific greenstone belts of the Proterozoic with most of its VMS clustered in the Snow Lake, Flin Flon, Birch Lake and Hanson Lake juvenile arc assemblages (Galley et al. 2007).

3D interpretation problems

The overall moderately to steeply dipping structures of the FFGC as recorded by geological mapping at surface, markedly contrasts with shallowly dipping structures inferred on LITHOPROBE seismic profiles from the Trans-Hudson transect at depth (> 3 km). Although this contrast in dip remains poorly understood, it may be explained by a crustal-scale detachment marked on seismic data as a transition between largely transparent zones with few curvilinear reflections on stacked mid- and deep crustal panels with strong east-dipping reflectivity (Lucas et al. 1993). Similar 3D interpretation problems at more local scale occur at higher upper crustal levels (depths < 3 km). The 3D model of the Flin Flon mine camp has revealed that structures, previously considered to represent arc assemblage-bounding subvertical shear zones with late strike-slip movement, turn out to be reactivated east-dipping thrust faults that align with crustal-scale shear zones marked by east dipping seismic reflectivity. These shear zones brought-up Flin Flon arc assemblage basement over Missi Group sedimentary cover, resulting in blind imbricates of juvenile arc basement within thrust-stacked Missi Group metasedimentary rocks. Moreover, thrust faults internally imbricated the Flin Flon arc assemblage, which resulted in repetition of felsic volcanic units hosting the Flin Flon VMS deposits (Schetselaar et al. 2016). 3D regional-scale modelling will address questions regarding outstanding geological interpretation and exploration targeting problems:

- Is post-Missi thrust-imbrication of lithostratigraphic units with the potential to host VMS deposits also significant in other structural domains (i.e., ‘fault blocks’) of the FFGC?

- Which of the thrust faults, active after deposition of the Missi Group, are reactivated structures that accommodated intra-oceanic accretion?

- Is the near-surface thick-skinned thrust and fold belt style of deformation confined at depth by a major subhorizontal decollement or do these structures root into the structures that accommodated stacking of the east-dipping mid- and deep crustal panels that apparently define FFGC basement?

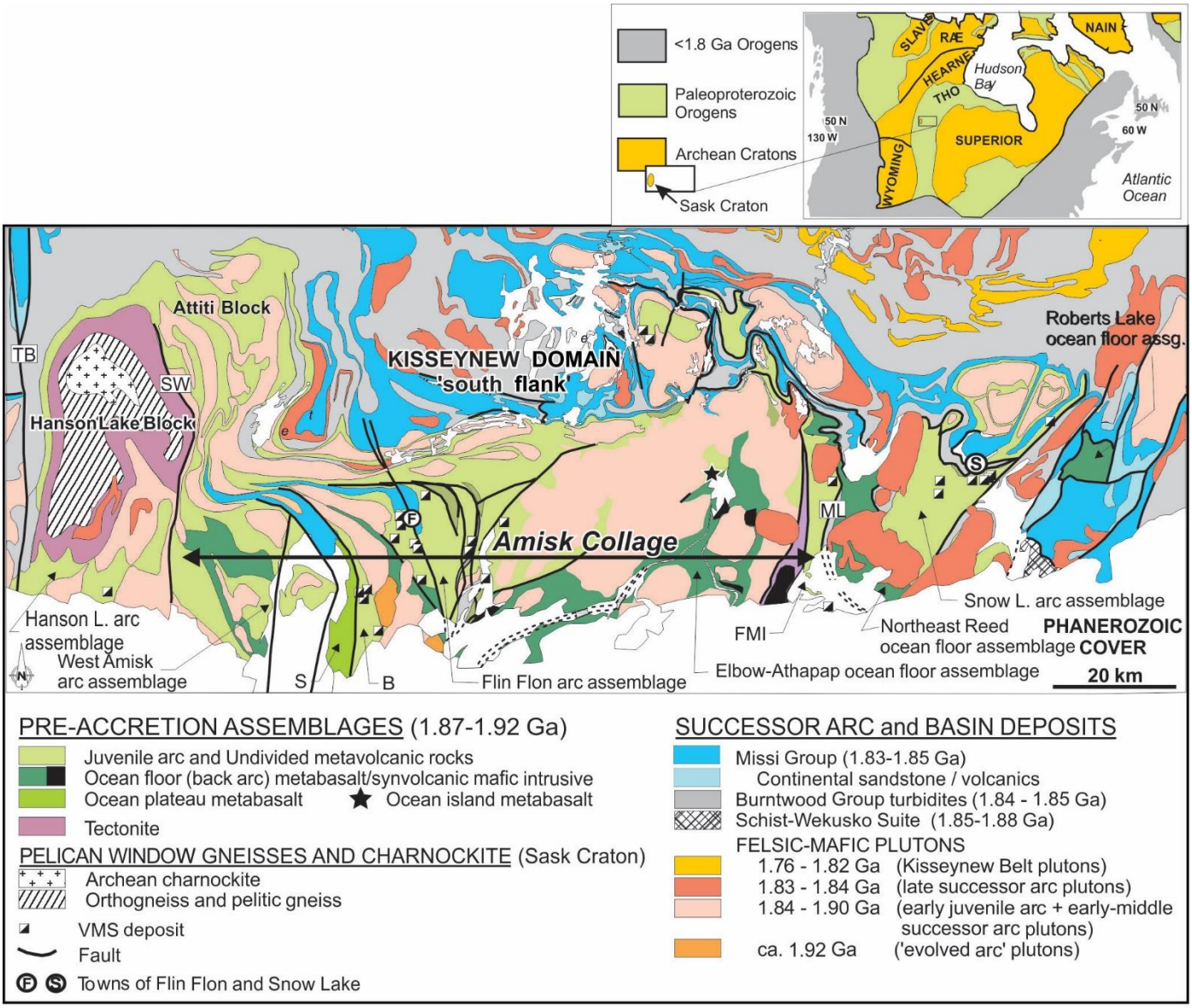

Figure 2 Tectonic assemblage map of the Flin Flon – Glennie Complex (after Galley et al., 2007 and references therein), illustrating the tectonostratigraphic assemblages, the location of the various accretionary assemblages, and major mineral deposits. B = Birch Lake assemblage; FMI = Fourmile Island assemblage; ML = Morton Lake fault zone; S = Sandy Bay assemblage; TB = Tabbernor fault zone. The box shows the location of the Flin Flon exploration camp.

- Can structural domains with thrust-stacking of drill-intersected felsic volcanic units with potential for hosting VMS deposits be identified?

- Can the relative positions between heat-generating synvolcanic plutons, regional alteration zones and massive sulfide deposits of VMS ore systems (Gibson et al. 2007) be restored for exploration targeting?

- Is there mineralization potential in areas that at surface appear to correspond to domains of plutonic and metasedimentary rocks, but at depth suggest the presence of blind thrust imbricates of juvenile arc assemblage rocks?

3D UNCONSTRAINED POTENTIAL FIELD INVERSION

Regional depth exploration in the FFGC of Manitoba and Saskatchewan requires the use of several ground and airborne geophysical methods, such as seismic, MT and potential field methods. Several geophysical interpretation studies using seismic, MT, aeromagnetic and gravity surveys have been conducted in this region under the auspices of the LITHOPROBE Trans-Hudson transect (THOT; Hajnal, 1995) and Shield Margin projects (NATMAP; Leclair et al. 1997). As part of the NATMAP program, the GSC has published a set of bedrock geological maps of the Flin Flon Belt, in which aeromagnetic and gravity data, allowed mapping the extension of exposed geological domains and regional structures below Phanerozoic cover (Leclair et al, 1997; NATMAP Shield Margin Working group, 1998). This NATMAP sub-Phanerozoic compilation was more recently revised by Simard and McGregor (2009) in Manitoba and Morelli (2012) in Saskatchewan. These authors used the publicly available and company-owned aeromagnetic and gravity data in combination with descriptive logs, geochemical and geochronological analyses of hundreds of drillholes to revise the major domains of the FFGC in the subsurface.

The regional data currently available are ground gravity data with an inter-station spacing of 4 to 6 km (Fig. 3a) and high resolution airborne magnetic data draped at 150 m elevation with a 75 m cell size resolution compiled by Ugalde (2019). This high-resolution aeromagnetic data covering the FFGC was merged to a 200 to 800 m resolution survey to obtain a more continuous dataset (Fig. 3b). All the data was interpolated using the minimum curvature algorithm in Geosoft. Herein, preliminary unconstrained density and magnetic susceptibility inverse models were generated to support 3D regional interpretation of the FFGC. Subsurface constraints from seismic and drillhole data will be integrated into the optimization objective function at a later stage. Figure 4 shows the magnetic total field data with an overlay of the NATMAP compilation of the exposed and shallowly buried portions of the FFGB to provide geological context.

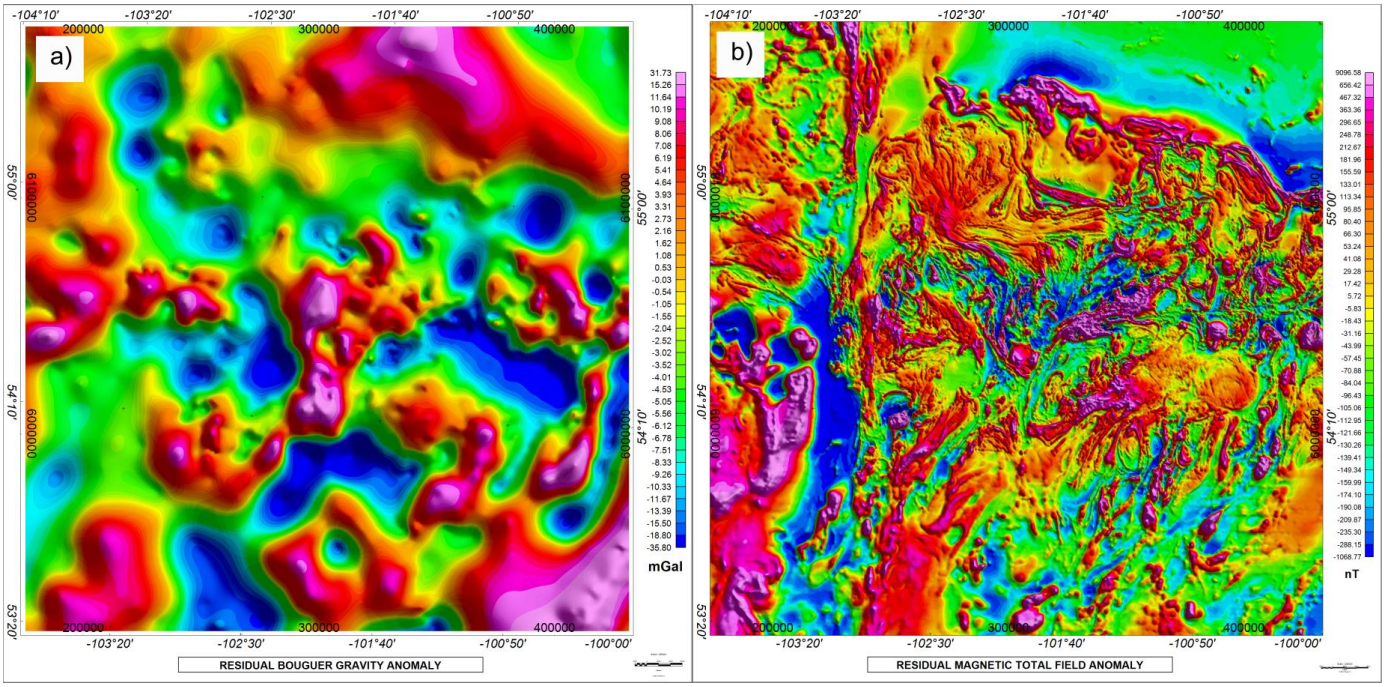

Figure 3 a) Residual Bouguer anomaly field in mGal (1 km grid). A regional trend was removed from the gravity data by using an upward continuation distance of 40 km. b) Residual magnetic total field anomaly in nT acquired at a height of 150 m above the ground. A regional linear trend was removed from the original magnetic dataset.

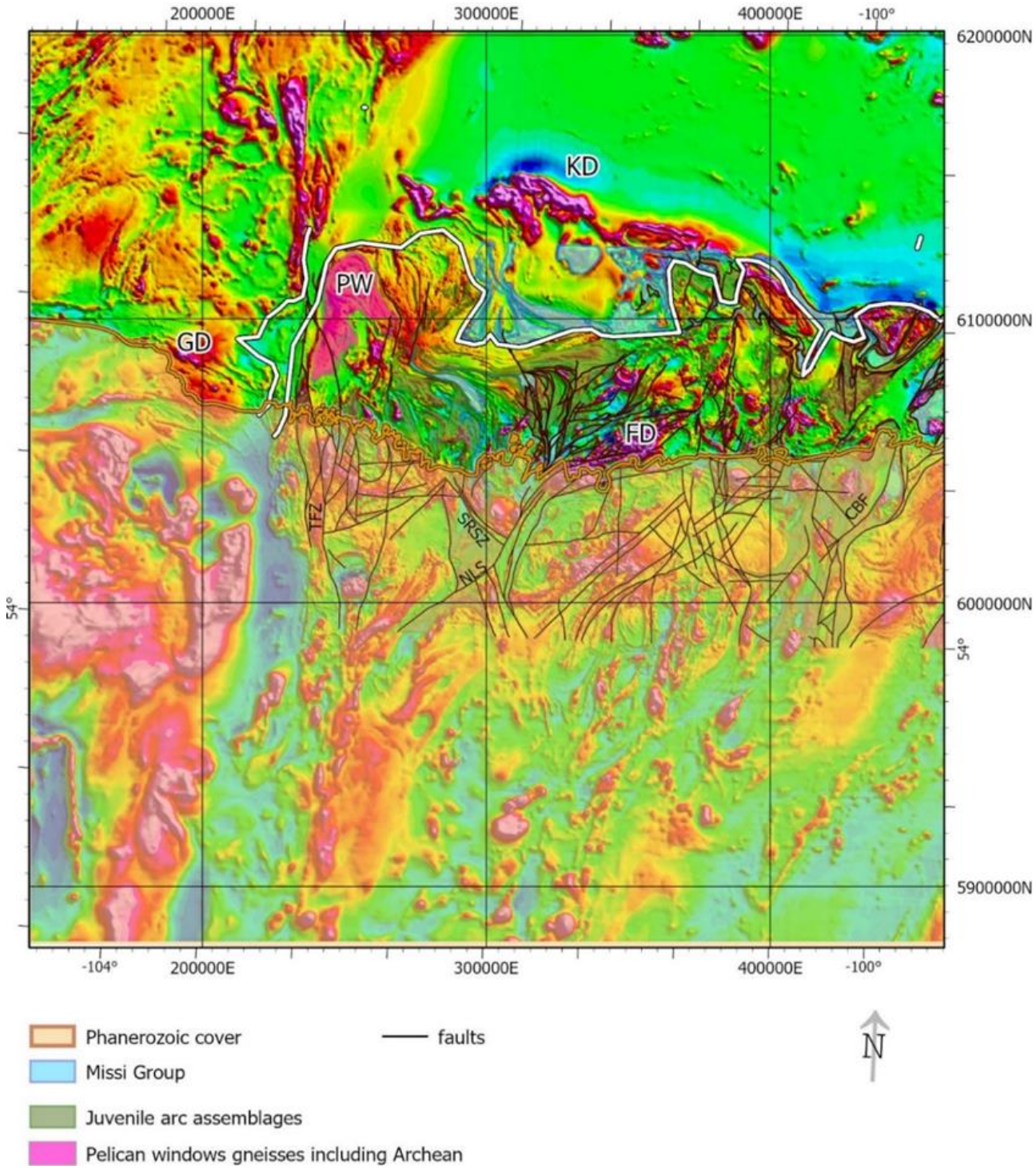

Figure 4 Geological domains draped over the total magnetic field grid covering the study area of Saskatchewan and Manitoba provinces. Main domains from the NATMAP project are represented by polygons of the Missi Group, juvenile arc assemblages and the Pelican window. The Phanerozoic cover south of the brown line include Paleozoic formations (Silurian, Ordovician). Interpreted faults (black lines) were compiled after the NATMAP project and Morelli, (2012). TFZ = Tabbernor fault Zone, SRSZ = Spruce rapids shear zone, NLS = Namew Lake structure, CBF = Crowduck Bay fault. FD = Flin Flon domain, GD = Glennie domain, KD = Kisseynew domain, PW = Pelican tectonic window.

A 3D unconstrained magnetic inversion was carried out in the Fourier Domain with sparseness constraints (Pilkington, 2009) using a mesh of 512 x 512 x 30 with 640 m cell size that was extended in x-y directions by 512 cells in the frequency domain to remove edge effects (Fig. 5). A 3D unconstrained gravity inversion was carried out in the space domain by using flatness constraints (Boulanger and Chouteau, 2001) using a mesh of 256 x 256 x 30 mesh with a 1000 m cell size (Fig. 6).

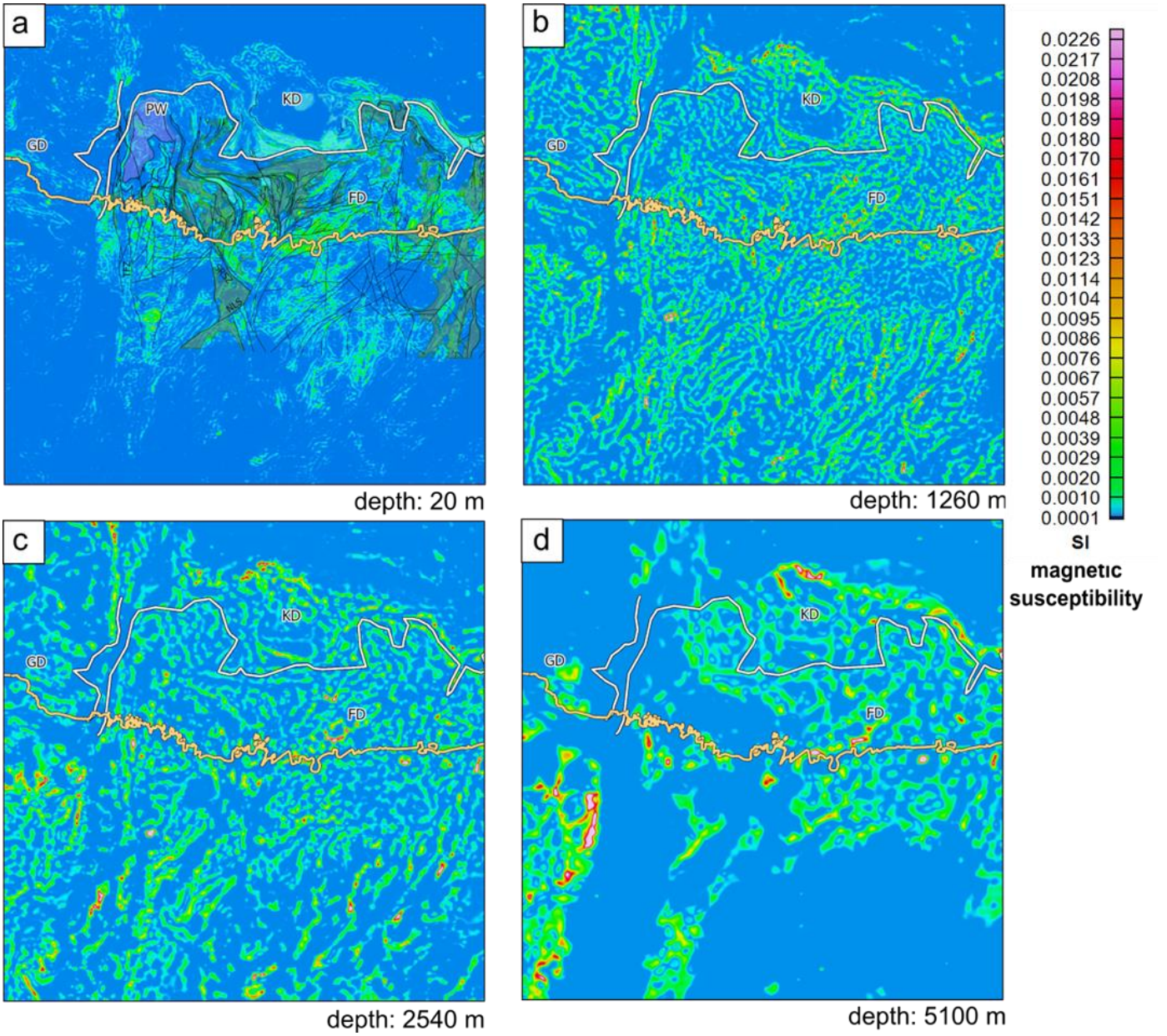

Figure 5 Plan views of the unconstrained magnetic inversion using magnetic airborne data presented in Figure 1b). The magnetic susceptibility in SI is presented for depths of a) 20 m, b) 1260m, c) 2540m and d) 5100 m. Regional geological domains and structures shown on Figure 5a correspond to the overlay shown in Figure 4.

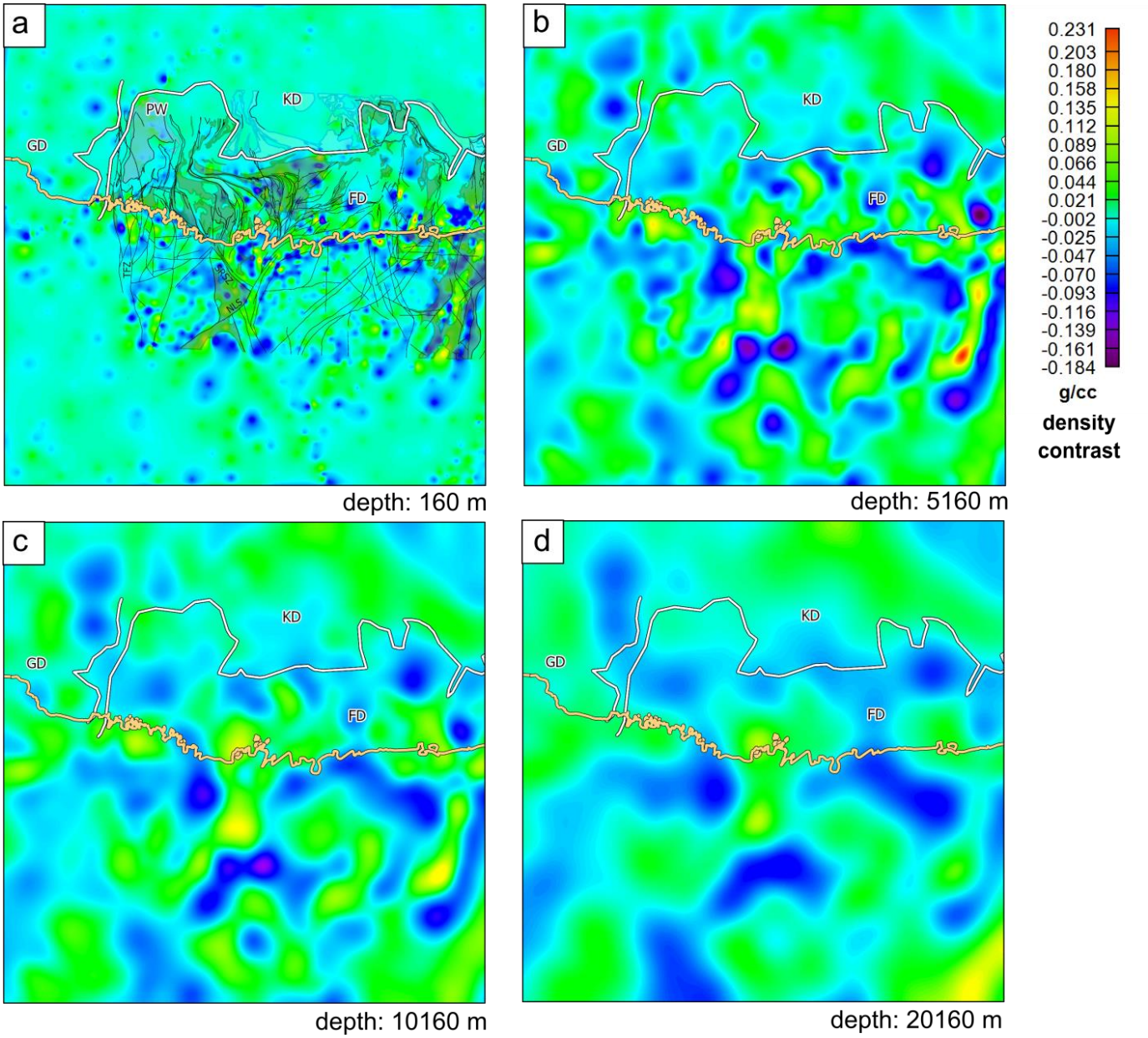

Figure 6 Plan views of the unconstrained gravity inversion using the ground gravity data presented in Figure 1a). The density in g/cm^{3}is presented for depths of a) 160 m, b) 5160 m, c) 10160 m and d) 20160 m. Regional geological domains and structures shown on Figure 6a correspond to the overlay shown in Figure 4.

The next steps will aim at adding several types of constraints such as physical rock properties, geometric constraints based on seismic information, and dip constraints measured at surface or estimated from drillhole data where available. This will allow interpreting the geological significance of the 3D density and magnetic susceptibility distributions. Integration of the self-demagnetization is another important step in the forward modeling and adjustment of the depth weighting.

3D INVERSION OF LITHOPROBE MAGNETOTELLURIC (MT) DATA

The objective of this project component was to provide a regional electrical resistivity framework to be used to bridge the gap between deposit-scale EM or MT studies to ore-system scale; and to aid in the evaluation of the utility of MT data to investigate sub-Phanerozoic geological features as a part of future TGI projects. The LITHOPROBE MT data herein are described in Jones et al. (2005) and a review of the 2D models is provided by Akaranta (2011). The new modeling technique we have utilized is ModEM (Kelbert et al. 2014). ModEM's inherent modularity and widespread community acceptance has proven the software to be a robust tool to examine MT data. Totaling over 700000 cells, the starting model created for this activity consisted of 45 x 274 x 57 (X, Y, Z) mesh elements spanning beyond the scope of the study area to include the entirety of the LITHOPROBE survey. To save computational resources, it is common practice in memory intensive 3D MT studies such as this to only invert a subset of the sites or periods measured. However, given NRCan's recent access to AWS all impedance and tipper data from all sites at all 50 periods (10000 Hz to 1820 s) from the combined LITHOPROBE AMT and AMT/MT data sets could be utilized for the analysis.

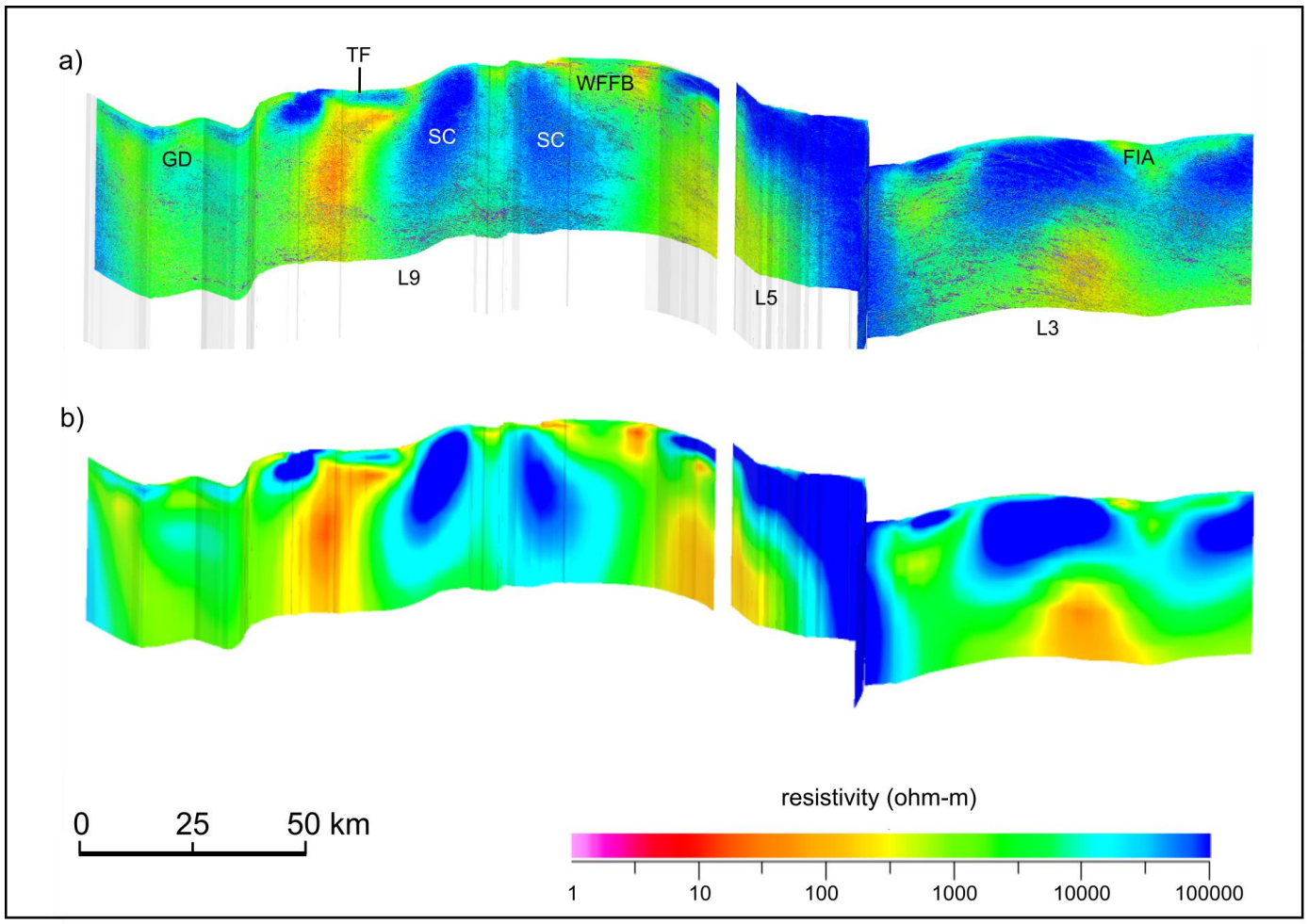

Figure 7 Vertical slices from the new 3D MT inverse model projected on LITHOPROBE lines 3, 5 and 9. a) inverse MT model merged with seismic amplitude; b) inverse MT model. The full model extends to 750 km depth, but only the upper 40 km is shown. The model slices have been smoothed to emphasize the large deeper features. GD = Glennie domain, TF = Tabbernor fault, SC = Sask craton, WFFB = Western Flin Flon belt, FIA= Fourmile Island assemblage.

This inversion could therefore be one of the, if not the largest, performed in terms of number of periods simultaneously inverted in MT at the time writing of this article. A rigorous appraisal of model resolution has not been conducted, but overall, the misfit to the data normalized by error is good (RMS = 1.75). The result of the inversion within the confines of the scoping project is shown in Figure 7. A preliminary interpretation of key features is also shown to aid in comparison with earlier 2D models.

One of these models from Ferguson et al. (2005) is shown in Figure 8. There are similarities between the earlier and present preliminary model, however the new 3D model better locates features or geometries predominantly associated with the north-south segment of the transect corresponding to the FFGC. Major features such as the Sask craton (labelled SC on Figures 7 and 8) are present in both images. A discrepancy however between the models at the Tabbernor fault zone warrants further investigation. Not labelled are the conductors on the eastern side of Figure 7, possibly related to the Athapapuskow Lake conductivity anomaly ALCA conductor mentioned by Jones et al. (2005). Confident correlation of these features is hampered by the sheer scale (size) of the models and comparatively small figure sizes in the literature. Further interpretation and correlations including collection and modelling of new data in the Amisk Lake region will be conducted during subsequent phases of the project.

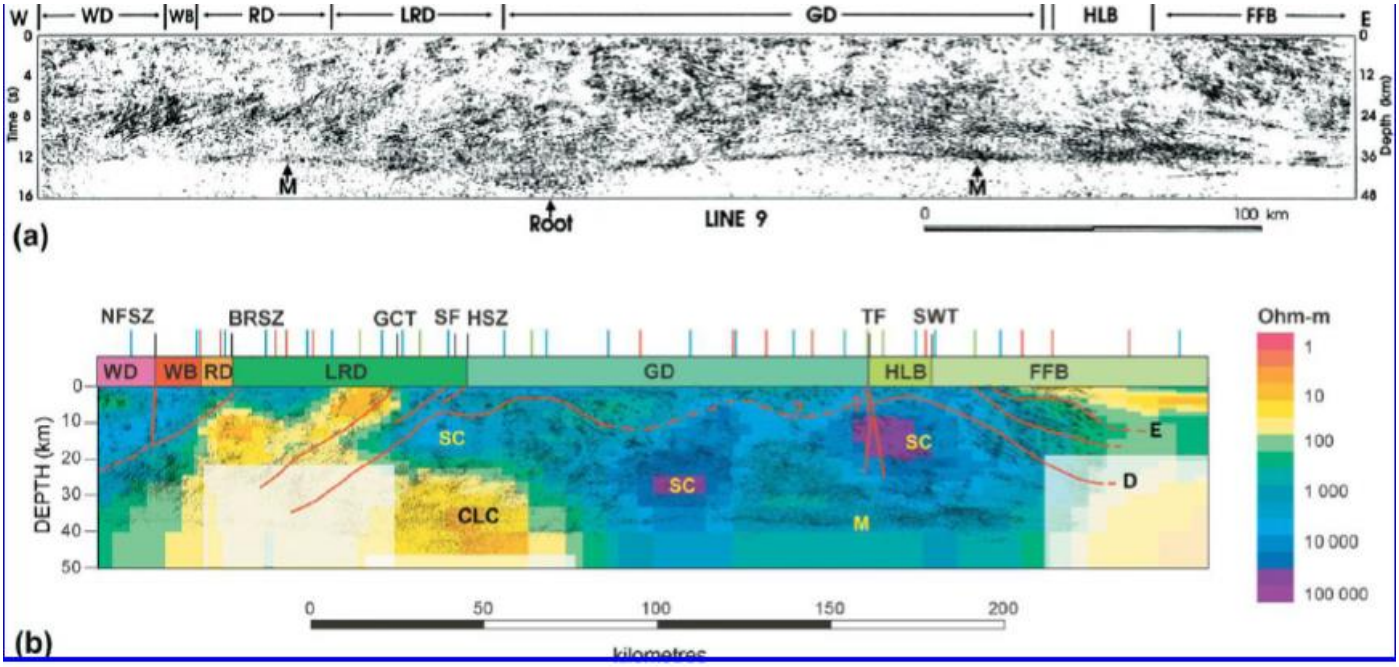

Figure 8 (a) LITHOPROBE seismic line 9 and (b) Legacy 2D MT inverse model combined with seismic reflectivity from Ferguson et al. (2005). WD = Wollaston domain, WB = Wathaman batholith, RD = Rottenstone domain, LRD = La Ronge domain, GD = Glennie domain, HLB = Hanson Lake block, FFB = Flin Flon belt, M = Moho, SC = Sask craton, CLS = conductive lower crust, NFSZ = Needle falls shear zone, BRSZ -= Birch rapid shear zone, GCT = Gun coat thrust, SF = Stanley fault, HSZ = Hartley shear zone, TF = Tabbernor fault, SWT = Sturgeon Weir tectonic zone.

PROGRESS ON 3D MAGNETOTELLURIC INVERSION ALGORITHM DEVELOPMENT

In conjunction with the TGI roadmap of realistic 3D geological mapping of complex ore systems and enhancement of deep geophysical exploration, this section discusses the theoretical development and use of a full-tensor three-dimensional (3D) magnetotelluric (MT) inversion/optimization algorithm that images Earth's electrical conductivity from surface to tens of kilometers of depth. For this purpose, a fully finite element (FE) based minimum structure inversion for the use on irregular (unstructured) meshes is developed. This is a novel methodology because both data misfit and regularization terms of the optimization objective function are treated using the relevant FE approximations that fully conform to irregularities of unstructured meshes. The inversion algorithm is coded based on the Gauss-Newton (GN) iterative optimization scheme with model perturbation being sought in each solution step. The algorithm is hyper-parallelized in OpenMP and MPI programming modes for a fast computation of finite-element functions in the forward solution engine, and for simultaneous implementation of the relevant sensitivity matrix calculations on multiple computing nodes/processors.

The traditional method of performing geophysical inversion on structured rectilinear (e.g., cubical) meshes lacks accuracy in fully capturing the irregularities of complex geological targets. This also can cause inaccuracies in producing the ideal EM response of electrical conductivity contrasts in the finite-difference based forward modelling tools. Unstructured meshes instead produce exact geometries of the subsurface and are flexible in incorporating various components of input constraints i.e., drillhole and pre-defined seismic horizons, through refinement strategies at the regions of interest. This provides a base towards producing a realistic geophysical response of any constructed model subject to using a suitable finite-element discretization scheme. The deterministic-type inversion methodology developed here is unique because the model roughness term of the Tikhonov objective function is fully treated using FE basis functions on irregular meshes that constrain explicitly a realistic variation of electrical conductivity across any geobodies included in the model.

The minimization of the objective function with respect to model perturbation in our inversion methodology led to the following equation:

$$(\mathbf{J}^{\mathrm{n-1^T}}\mathbf{W}_{\mathrm{d}}^{\mathrm{T}}\mathbf{W}_{\mathrm{d}}\mathbf{J}^{\mathrm{n-1}} + \lambda^{\mathrm{n}}\alpha_{\mathrm{m}}\mathbf{S}^{\mathrm{T}}\mathbf{M}^{-1}\mathbf{S})\ \delta\mathbf{m}^{\mathrm{n}}$$
$$= \mathbf{J}^{\mathrm{n-1^T}}\mathbf{W}_{\mathrm{d}}\mathbf{W}_{\mathrm{d}}(\mathbf{d}^{\mathrm{obs}} - \mathbf{d}^{\mathrm{n-1}}) - \lambda^{\mathrm{n}}\alpha_{\mathrm{m}}\mathbf{S}^{\mathrm{T}}\mathbf{M}^{-1}\mathbf{S}\ (\mathbf{m}^{\mathrm{n-1}} - \mathbf{m}^{\mathrm{ref}})$$

Which is a GN least-square type system solved for the model perturbation δm. J and W are the data sensitivity and weights, λ is a trade-off parameter, and m serves as a parameter for incorporating initial, inverted and reference models. The novelty of the formulation developed here is the FE approximation of smoothing parameters S and M with the innovative design of mesh-size-independent gradients that account for non-zero jumps of the model gradient across the inter-element boundaries of unstructured tetrahedral cells. For this gradient-based FE basis functions were designed and discretized on tetrahedral meshes, and subsequently coded into the inversion algorithm. The algorithm was validated for benchmark examples from the literature and its computational efficiently is also being tested. The test for the inversion of data from the regional-scale Commemi 3D-2A model (Fig. 9) was performed for the full impedance tensor, and for 32 frequencies ranging from 0.00005 to 60 Hz. The inversion results confirm the anticipated recovery of the true model subject to starting the optimization algorithm with a number of initial model inputs (Fig. 10). In particular, the inversion with an initial half-space model of 0.1 S/m (Fig. 10 a, b and c) recovered the first layer and the surface anomalous targets but showed weakness in imaging the ideal geometry of the second and third layers. Starting the

inversion with an initial model constructed from the interpolation of 1D inversion of the impedance data (its averaged root mean square) into the mesh recovered fully the layering and conductivity of all features (Fig 10 d, e, and f). This demonstrated the importance of starting the inversion with a model that is as close to the true model, and the final inverted model ensures a reliable image recovery at the deeper parts and to the sides of the model.

The Lalor VMS deposit, located in the Snow Lake domain of the FFGC (Fig. 1, area 2) was used as a case study to test the performance of the inversion algorithm. We previously studied the forward MT response of this deposit by developing realistic electrical resistivity models from on-site lithostratigraphic and drill-hole data (Ansari et. al., 2020). Figure 11 shows one of these lithostratigraphic conductivity models generated by computing sequential Gaussian simulations from drillhole resistivity logs for each class of a 3D lithofacies curvilinear grid model (Schetselaar et al., 2018). This curvilinear grid model was subsequently resampled to the unstructured tetrahedral mesh (Ansari et al., 2020, Fig. 11a). It is geologically realistic in the sense that it honours lithostratigraphic controls, as well as the heterogeneous distribution of sulfide mineralization, the latter being evident in the drillhole resistivity data. Impedance data for this model was computed for 24 frequencies (0.0054–15000 Hz) and polluted with gaussian noise to test the resolvability of the inversion algorithm. Figure 11b shows a zoomed view of the mesh that was used for the inversion experiment. It has the same scale and dimensions as the resistivity model (Fig. 11a).

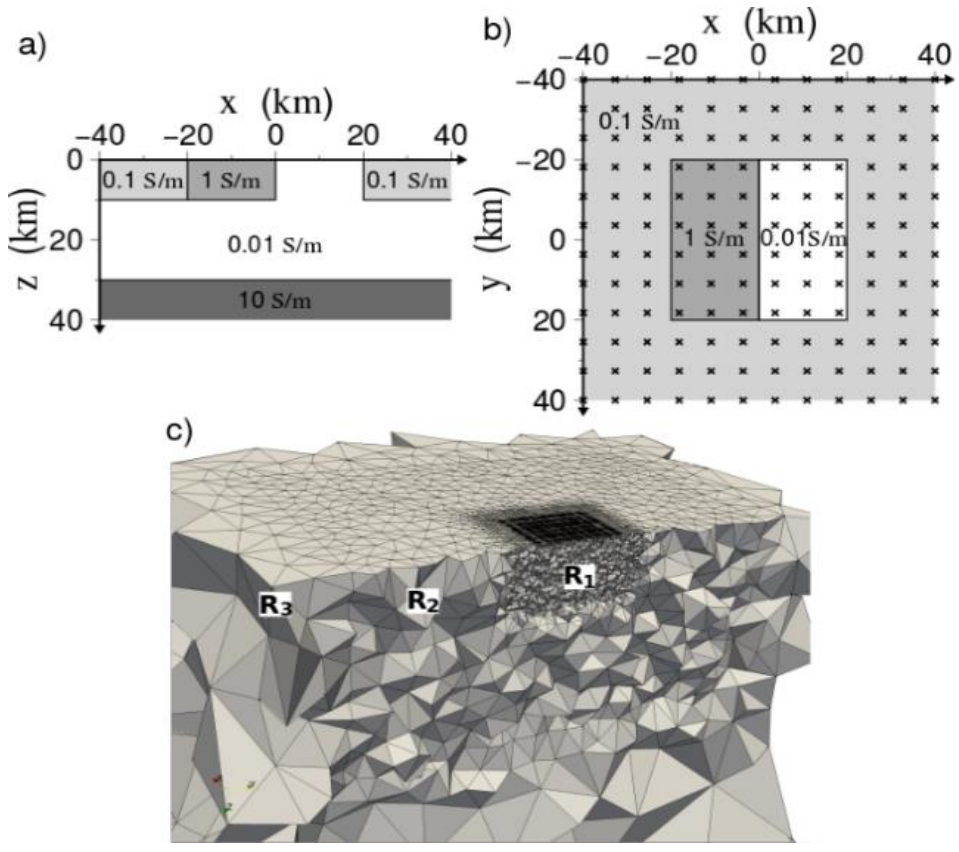

Figure 9 Vertical (a) and horizontal (b) cross section views of the Commemi 3D-2A model, with observation locations (MT sites) shown in crosses symbols. c) The unstructured mesh with three refinement regions (R1, R2, and R3) used for the inversion.

The total number of cells in this mesh is 363011. Starting with a trade-off parameter of 105 that was reduced with a factor of 0.75, the inversion was initiated with 0.0005 S/m a-priori and reference models. The algorithm was deemed converged if the minimum data misfit or a minimum trade-off parameter of 100 was reached, whichever preceded. The model was then smoothed further for more iterations. Figure 12a shows the inverted model after 40 GN updates. Figure 12b shows a 2D slice through the central profile. The inverted model has clearly reproduced the resistive to conductive sequence of footwall and hanging wall lithostratigraphic units of the conductivity model (Fig. 11a). By comparing the synthetic and inverted models in a zoomed-in scale (Fig. 12c and Fig. 12d) the MT inversion has successfully produced the structure of the ore deposit despite the relatively coarser mesh used for the inversion. Constraining the inversion with initial models from 1D inversion, and with the stochastic procedure described above are the subject of upcoming studies in inverting for the real MT data collected in this area.

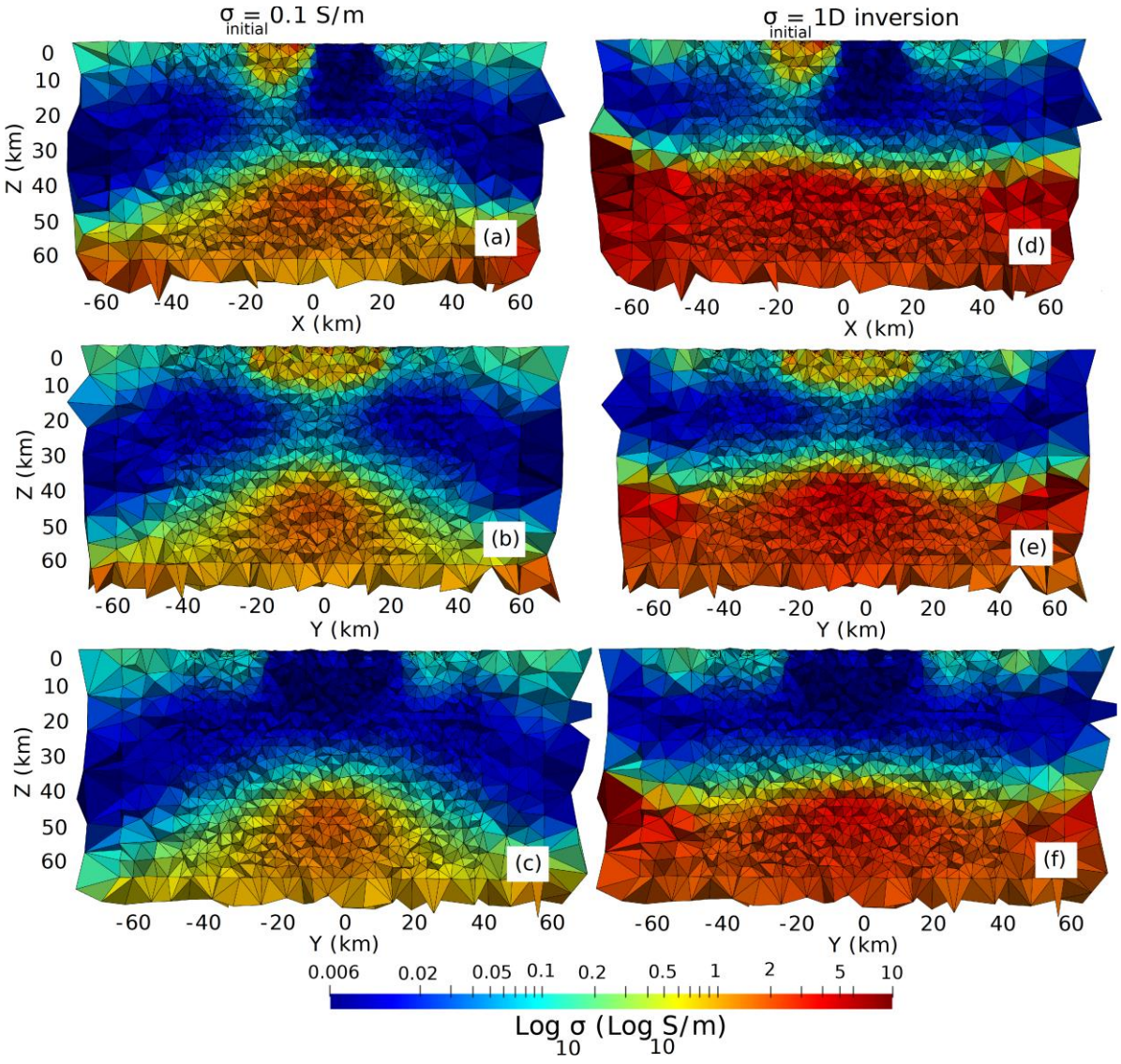

Figure 10 Vertical sections through the inverted model for runs started with initial models of 0.1 S/m, and 1D inversions merged into the mesh. These are for a selection of slices at x = 2.5 km (a and d), y = -10 km (b and e), and y = 10 km (c and f).

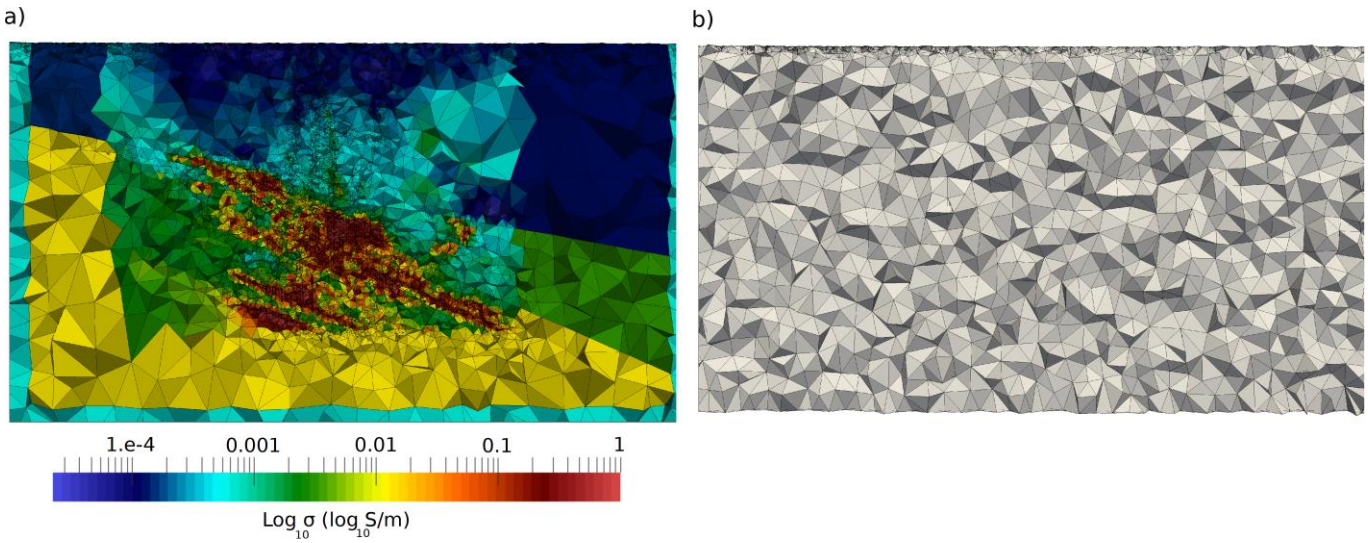

Figure 11 a) Stochastic conductivity model of the Lalor ore deposit used for producing the pseudo-realistic MT forward modelling data. b) Comparable view of the mesh used for the first inversion experiment.

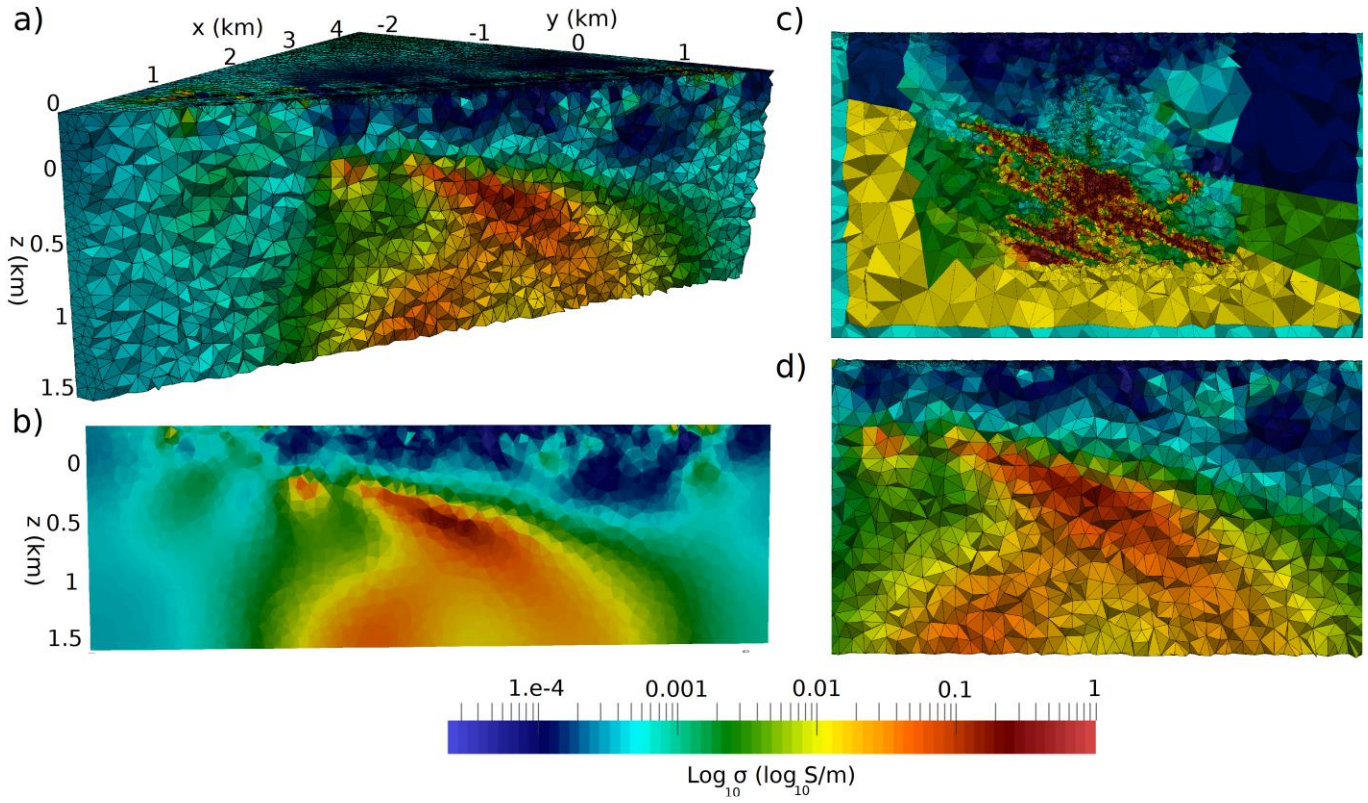

Figure 12 a) A crinkled pseudo 3D slice from the central profile in the final inversion model after 40 GN updates. b) 2D slice of the central profile extracted from a). c) The constructed lithostratigraphic conductivity model (same as Fig. 11a) from which the synthetic survey data is produced. d) Inverse model for the same view as shown in c.

NEW ACQUISITION AND RE-PROCESSING OF SEISMIC DATA

The Flin Flon Belt has been the subject of several seismic data acquisition programs, including the Trans-Hudson LITHOPROBE transect, high-resolution seismic profiling and 3D seismic surveying in the Flin Flon and Snow Lake mining camps. In this project, the LITHOPROBE seismic data are used primarily to define large regional domains in the crust (see the section below on the preliminary crustal model). Still, they will also provide helpful information at shallow depths to improve ties with surficial geology. To this end, selected areas of the LITHOPROBE lines will be the subject of a re-analysis and re-processing aiming to strengthen ties with surface geology. However, the areal coverage of the legacy seismic data is limited and lacking in some key areas of the 3D model. As part of this project, a 2D seismic profile was acquired to provide geological information west of Flin Flon along the eastern side of Amisk Lake and south of the Sturgeon River (Fig. 13). This subsection provides details on this new seismic data acquisition and the re-analysis of the LITHOPROBE data.

2D seismic data acquisition near Denare Beach

A 60 km long 2D seismic profile was acquired in February to March 2021 to add new geological constraints to the 3D model east and south Amisk Lake. This area was chosen for new seismic acquisition for several reasons: 1) it overlaps with this rich multidisciplinary geophysical data set, including recent airborne geophysics surveys acquired in 2018 (magnetics, EM, and gravity gradiometry), 2) it is a priority area for Saskatchewan and Manitoba geological surveys, 3) it lies directly south from the Flin Flon camp which is host to extensive geological/geophysical information.

Figure 13 Location of the recently acquired Denare Beach 2D seismic profile. The profile is divided into three parts, each having different surface conditions (see details in the text).

The 2D seismic profile was acquired with vibroseis and dynamite energy sources, with the intent of producing seismic images of the subsurface to depths of 10–15 km. Seismic data acquisition was performed by SAExploration when COVID-19 related restrictions were in place. Appropriate measures preventing COVID-19 propagation were implemented, and the seismic data acquisition was completed with no COVID-19 cases.

The profile is divided into three segments, each having different surface conditions. The first segment was acquired on a paved road (Highway 167) between Creighton and Denare Beach (Fig. 13). This segment had heavy traffic at peak hours and is close to residential neighbourhoods, especially near Creighton and Denare Beach. Data acquisition for that segment was conducted during the night to minimize disturbance to local traffic. The second segment follows the less travelled and inhabited portion of Highway 167 between Denare Beach and the end of the road at the Sturgeon River. Surface conditions for this segment consist of compacted gravel. The last segment is located south of the Sturgeon River along an old bush trail, which had to be partly cut due to regrown vegetation.

The data acquisition was performed in the winter, as an ice road across Amisk Lake was necessary to access the profile south of the Sturgeon River. Access over swampy areas on that segment of the profile was also facilitated with frozen ground. Segments 1 and 2 were acquired with vibroseis trucks, whereas explosives were used for the segment south of the Sturgeon River. The survey comprises 3391 shot points (2974 with vibroseis and 417 with dynamite) and 5,126,046 traces. The optimal vibroseis sweep was determined from tests conducted near Creighton before the survey. We opted for a 28 s linear sweep with frequencies ranging from 5–125 Hz. Source effort south of the Sturgeon River consisted of 2 kg explosives placed in 10–15 m shot holes tamped with bentonite and water. Source spacing varied from 12.5 m to 25 m (see Table 1) depending on the source type and operational constraints related to permits obtained to acquire data along Highway 167. Wireless seismographs/geophones (Oyo GSXs) synchronized with GPS time were placed over the entire profile with a spacing of 12.5 m. This comprises nodal geophones placed up to the intersection of the main roads in Creighton (i.e., highways 106 and 167) to allow ties with LITHOPROBE line 9. Record length was 8 s with a 2 ms sampling rate. Detailed survey parameters are presented in Table 1. Data quality varies significantly along the profile, but first breaks are generally observed to the largest offsets. This is an indication that source effort was sufficient. Shot gathers with clear reflections are observed on either side of the Sturgeon River for both vibroseis and explosive sources.

Table 1 Seismic data acquisition parameters.

Sources:	
Vibroseis truck (segments 1 and 2):	Two Sercel Nomad 65 Neo with a combined peak force 556 kN (124,800 lbf)
Sweep:	28 s linear sweep (5-125 Hz)
Explosive (segment 3):	2 kg in 10–15 m shot holes
Source spacing:	25 m between Creighton-Denare Beach 12.5 m between Denare to Sturgeon 25 m south of the Sturgeon River
Receivers:	
Receiver type:	Oyo GSX with vertical geophone
Receiver spread and spacing:	Symmetric spread with 1600 channels spaced every 12.5 m
Maximum offset:	10 km
Record length and sampling rate:	8 s at 2 ms
Nominal fold:	approximately 900 in the central part of the profile

Brute stack

Shot gathers near Creighton have weaker and less discernible reflections similar to other seismic data acquired previously in this area. The processing of the new 2D seismic data is currently in progress. A brute stack section obtained with a basic workflow (Table 2) and uniform processing parameters is shown in Figure 14. The area near the Sturgeon River already shows many reflections and diffractions (between CDP 2000–4000) with this minimalistic workflow. Reflections are observed down to 7.2 s (approximately 21 km) in this area of the brute stack (Fig. 14). Other profile areas contain weaker and less continuous reflections indicating that careful processing is necessary to produce a high-quality image of the subsurface. In particular, static corrections needed to mitigate the slowing and distorting effects of the unconsolidated weathered layers near the surface will be critical for improving the continuity of reflections on stacked and migrated sections. Effective static corrections depend primarily on picked times of first arrivals (or first breaks) on seismic records. In this project, first breaks are selected with a Deep Learning predictive tool developed specifically for this task as part of a collaborative project between GSC/Mila (St-Charles et al., 2021). This deep learning tool based on image segmentation improves the consistency of picks compared to classical trace-by-trace methods, especially for traces with a low signal-to-noise ratio.

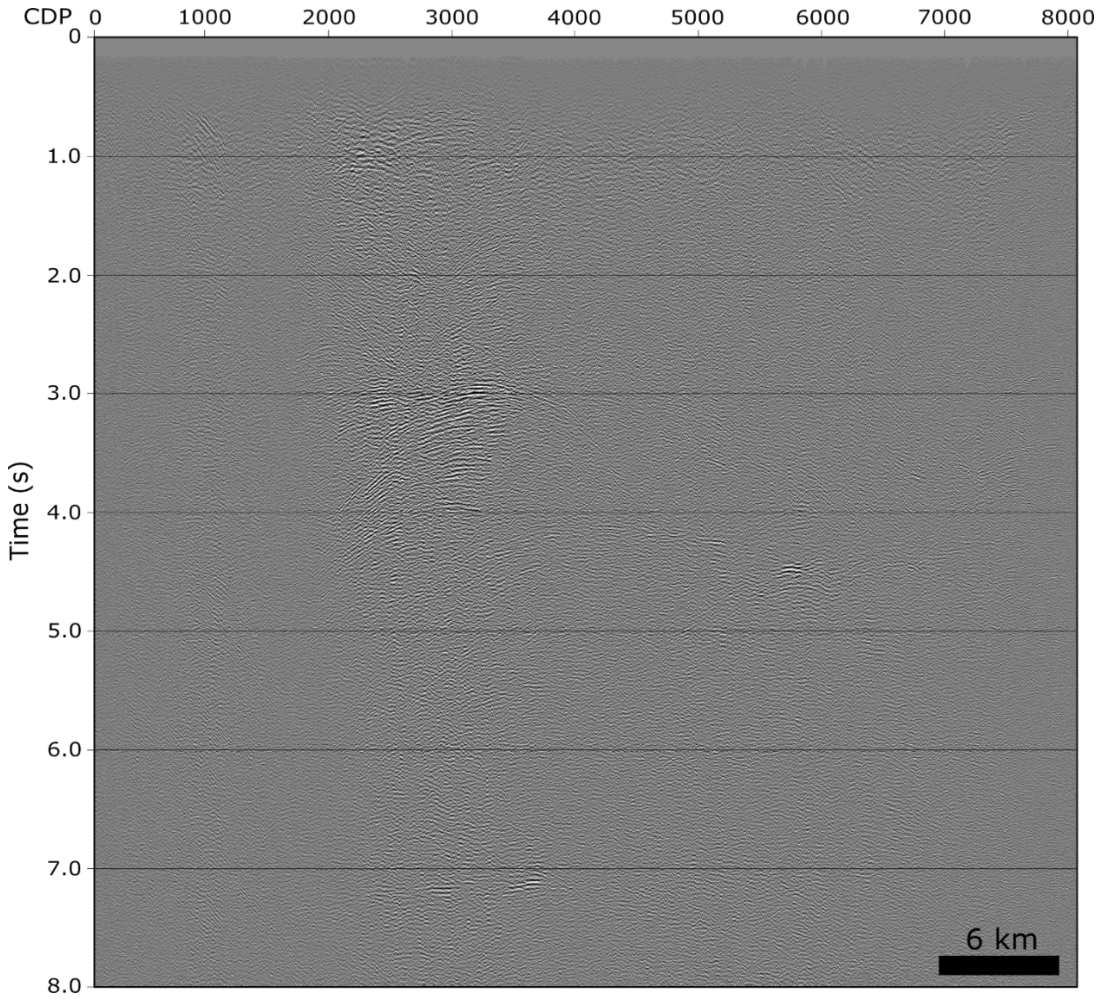

Figure 14 Brute stack of the Denare Beach 2D seismic profile obtained with processing parameters listed in table 2. CDP 0 is at the south end of the profile whereas CDP 8000 is near Creighton. Nominal CDP spacing along a crooked line geometry is 6.25 m.

Table 2 Processing parameters for the brute stack shown in Figure 14.

Spectral Equalization	15, 25, 90, 125 Hz
Automatic Gain Control	500 ms window
Muting of first breaks and above based on linear moveout velocity	Linear moveout velocity of 5750 m/s
Surgical S-wave muting based on linear moveout velocity	Linear moveout velocity of 3175 m/s
Elevation statics to fix elevation datum	Datum: 350 m Replacement velocity: 6000 m/s
A single velocity function for NMO corrections	5900 m/s at 0 s 6200 m/s at 8 s
Standard stacking	

However, predictive picking models are sensitive to numerous factors (source types, sampling rate, type of noise) and need to be trained with representative seismic data and labels (i.e., first break picks).

Re-analysis of LITHOPROBE seismic data

Some of the LITHOPROBE lines of the Trans-Hudson transect had high-quality data that provided excellent subsurface images. In particular, the western end of the east-west line 3 (Fig. 15) and the southern end of the north-south line 5 exhibit spectacular reflectivity, which can help make correlations with surface geology and contribute to building interfaces of the 3D model. However, most LITHOPROBE lines rarely show such a level of detail at shallow depths, primarily because processing focused on the entire section rather than only part of sections near the surface. As correlation with surface geology is an important aspect of this modelling project, a subset of the LITHOPROBE seismic profiles will be the subject of a targeted re-analysis and re-processing aiming at providing better images of the shallow geology and improving correlation with borehole and surface geology data in selected areas of the 3D model. The exact nature of the re-analysis and re-processing is still being discussed.

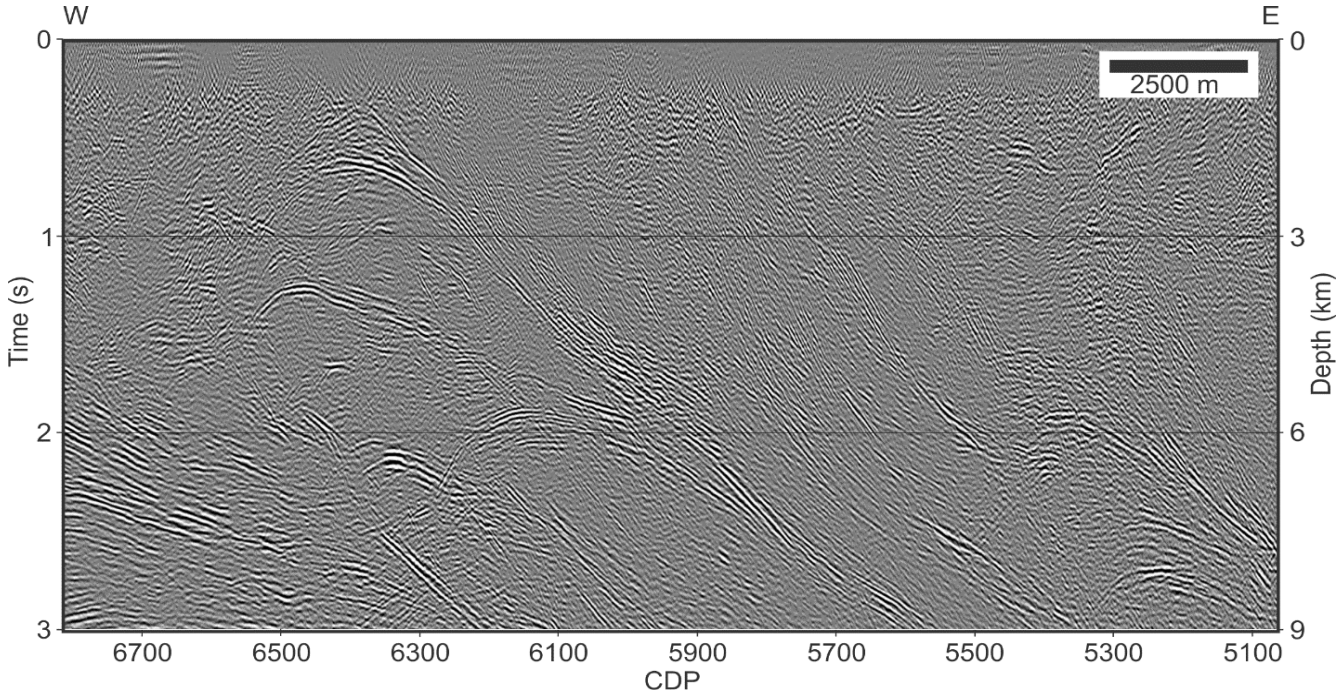

Figure 15 Western end of LITHOPROBE line 3 (migrated) showing spectacular reflections suggestive for fold-and-thrust-belt structural styles in the top 9 km.

3D DRILL HOLE - BEDROCK COMPILATION OF THE FLIN FLON MINING DISTRICT

One of the main challenges of integrated geological-geophysical modelling of the complexly deformed FFGC is to reconcile geological data from the surface and shallow subsurface (0–2 km) with deeper geophysical signatures. This requires systematic harmonization of the surface and subsurface geological data itself, which involves recoding lithology drill logs into generalized categories, representative for the regional-scale bedrock map pattern. Herein, we report a drill log recoding methodology for matching industry drillhole lithology logs with the cross-provincial NATMAP bedrock compilation of the FFGC (NATMAP Shield Margin Project Working Group, 1998) from a 25 x 25 km^2 test area around the Flin Flon mine camp (Fig. 16).

Previous camp- and regional scale 3D modelling projects conducted by the GSC demonstrated the value of generating lithostratigraphic interpretations of preselected drillholes to support 3D geological modelling (Schetselaar et al. 2016; de Kemp et al., 2017). The classification of the numerous lithofacies units recognized in drill core into a significantly lower number of laterally persistent lithostratigraphic categories, spatio-temporally ordered according to rules of stratigraphic superposition or intrusion, enforces the generalized lithostratigraphic drillhole compilation to be consistent with the knowledge acquired in regional bedrock mapping campaigns. Because the drillhole interval lithostratigraphic interpretations are harmonized with the legends of geological maps, drillhole markers can be matched with their corresponding contacts at surface so that their 3D alignment can established and subsequently traced into the subsurface (Fig. 17).

In this contribution, we extend this lithostratigraphic drillhole recoding approach to tectonostratigraphic assemblages and post-accretionary intrusive suites compiled on the NATMAP bedrock compilation of the FFGC. These units include juvenile arc assemblages, oceanic plateaus, continental and marine sedimentary basin sequences and post-accretionary granitoid and mafic intrusive suites (Table 3). Although recoding logged lithofacies into the most general units of the lithostratigraphic-lithodemic classification hierarchy obviously leads to extreme levels of generalization and carries over compilation uncertainties, it is envisaged that the drillhole markers defining their contacts are better reconcilable with reflections from regional-scale seismic profiles (Fig. 18) potential field and MT inverse models. Obviously, dependent on the objective of the interpretation, more detailed levels of the classification can be included if higher-spatial resolution details are evident in geophysical data and/or models. Regardless which classification level is used, follow-up drill core logging of selected holes, aided by interpretation of whole-rock major oxide and trace element geochemistry is essential for validating and refining these preliminary interpretations.

The following data processing steps were employed in recoding the industry-logged lithology intervals:

1. Selective retrieval of all drillhole database records (collar, deviation and lithology logs) with a path length equal to or exceeding 500 m.
2. Clean up formatting errors such as discrepancies in total length between collar and deviation log database records and sorting errors in lithology and deviation logs.
3. Drillholes without deviation logs were approximated using straight drill paths by generating pseudo deviation logs from the drilled length, azimuth and dip collar records.
4. The study area was subdivided in fault-bounded tectonostratigraphic domains where encoding of drillhole intervals to geological map units can be universally applied with reasonable certainty. These domains included the Flin Flon arc assemblage, the Hook Lake Block and ocean floor domains (Fig. 16).

5. Lithologic codes were translated into tectonostratigraphic intervals of the NATMAP bedrock compilation applying a recoding schema for the major tectonic domains in the test area (Table 3). A code for felsic volcanic intervals in the juvenile arc assemblages (Jf) was added to the schema because these intervals are expected to contrast significantly with the density and acoustic impedance of the other units of the juvenile arc assemblages that are dominantly mafic in composition. As a result, the contacts between felsic volcanic and volcaniclastic intervals and units of mafic composition have elevated potential to generate reflections on regional seismic profiles.

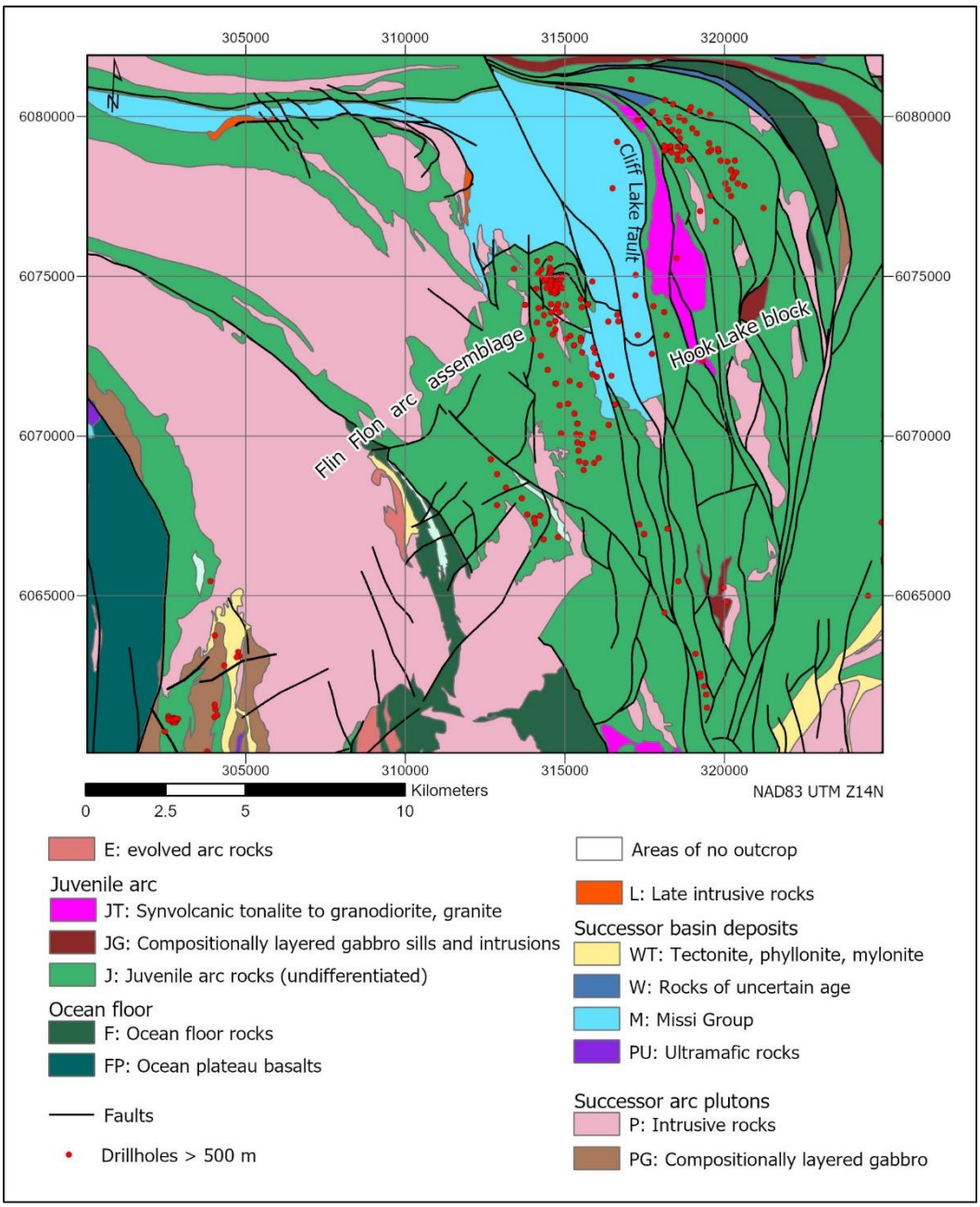

Figure 16 Generalized compilation of the NATMAP bedrock map (NATMAP Shield Margin Project Working Group, 1998) of the area in which harmonized encoding of drillhole and bedrock geological map data was tested.

Table 3. Classification schema for recoding industry-logged lithology drillhole intervals into generalized map units of the NATMAP bedrock compilation (NATMAP Shield Margin Project Working Group, 1998). Units colour code correspond to legend of the generalized NATMAP compilation (Fig. 16).

Drillhole lithology intervals	Generalized NATMAP unit description (assemblage, group, suite level)	NATMAP code	Drillhole code
Flin Flon arc assemblage			
Felsic volcanic and volcaniclastic rocks	Juvenile arc assemblage, felsic units	J	Jf
All other volcanic rocks and mineralized argillite	Juvenile arc assemblage	J	J
Mafic intrusive rocks	Compositionally layered gabbro sills and intrusions	JG	JG
Felsic intrusive rocks	Successor arc felsic intrusive units	P	P
Mafic intrusive rocks	Successor arc mafic suite	PG	PG
Ultramafic rocks	Successor basin deposits (ultramafic rocks)	PU	PU
Coarse clastic metasedimentary rocks (conglomerate, sandstone)	Successor basin deposits (Missi Group)	M	M
Sheared and mylonitized metasedimentary rocks	Successor basin deposits (tectonite, phyllonite, mylonite)	WT	WT
Ductile shear			SHR
Brittle shear / fault			TF
Hook Lake block			
Felsic volcanic and volcaniclastic rocks (rhyolite-dacite)	Juvenile arc assemblage, felsic units	J	Jf
All other volcanic and volcaniclastic rocks and mineralized argillite	Juvenile arc assemblage	J	J
Mafic intrusive rock (classified on spatial context bedrock map units)	Compositionally layered gabbro sills and intrusions	JG	JG
Felsic intrusive rocks (tonalite, granodiorite, granite; classified on spatial context bedrock map units)	Synvolcanic felsic intrusive units (Cliff Lake pluton)	JT	JT
Felsic intrusive rocks	Successor arc felsic intrusive units	P	P
Mafic intrusive rocks	Successor arc mafic suite	PG	PG
Coarse clastic metasedimentary rocks (conglomerate, sandstone)	Successor basin deposits (Missi Group)	M	M
Clastic metasedimentary rocks (conglomerate, sandstone, siltstone, argillite)	Successor arc basin deposits	W	W
Sheared and mylonitized metasedimentary rocks	Successor arc basin deposits (tectonite, phyllonite, mylonite)	WT	WT
Ductile shear intervals			SHR
Brittle shear / fault intervals			FLT
Ocean floor			
Mafic igneous rocks (classified on spatial context bedrock units)	Ocean floor rocks	F	F
Mafic igneous rocks (classified on spatial context bedrock units)	Ocean plateau basalt	FP	FP

6. Thin (< 15 m) 'FROM-TO' intervals were merged with adjacent intervals by assigning the tectonostratigraphic code of the intervals above and/or below the interval considered. Faulted and sheared intervals thinner than 15 m were left intact to maintain the capacity to establish hole-to-hole correlation for faults and shear zones.
7. Adjacent drillhole intervals with the same NATMAP tectonostratigraphic drillhole code were merged into single 'FROM-TO' intervals.
8. Lithostratigraphic coding errors and inconsistencies recognized in the joint 3D visualization of the encoded drillholes and NATMAP bedrock geological map were corrected.

Preliminary regional-scale 3D interpretation

Figure 19 shows 3D visualizations of different viewing perspectives of the harmonized drillhole-bedrock compilation. Note that the majority of the drillholes, including the deepest drillholes, cluster around the Flin Flon and Trout Lake mine camps. The following section presents 3D visualization examples of the harmonized compilation providing new 3D insights into the regional subsurface architecture of the Flin Flon arc assemblage.

Regional thrust imbrication of Missi Groups metasedimentary rocks

Camp-scale 3D modelling at Flin Flon demonstrated that the Missi Group metasedimentary cover does not, as was previously shown to define the core of an intact structural synclinal basin on a schematic east-west cross section (unpublished diagram HudBay Minerals Inc.) but is imbricated with juvenile arc assemblage basement by west-verging thrust faults (Schetselaar et al. 2016). The harmonized bedrock-drillhole 3D compilation presented here corroborates this interpretation and suggests that the thrust imbrications are also regionally significant. Aligned contacts between volcanic basement rocks in the hanging wall and Missi Group metasedimentary rocks in the footwall show regional scale thrust imbricates of unit J on at least three structural levels (Fig 20):

- SL1: Fault contacts between conglomerate and sandstone of the Missi Group and mafic volcanic and volcaniclastic rocks of the Flin Flon arc assemblage. These faulted contacts occur a few hundred meters below thrust repeats of the massive-sulfide hosting Millrock member in the footwall and hanging wall of the Flin Flon Lake fault (Fig. 20, Schetselaar et al. 2016) a structural feature of the third deformation phase (Lafrance et al. 2016). Discontinuities in the alignment of the Missi Group drillhole markers (Fig. 20) are due to displacements of these faults by north-vergent thrust faults, which are structural features of the fourth deformation phase (Lafrance et al. 2016).

- SL2: Basal thrust imbricate of hydrothermally altered mafic volcaniclastic and volcanic rocks between panels of Missi Group metasedimentary rocks. A small portion of this imbricate is exposed in the Lake view showing (Simard et al. 2010).

- SL3: Cliff Lake fault that defines the contact between the Flin Flon arc assemblage and Missi Group sedimentary cover with the volcanic rocks of the Hook Lake Block and the synvolcanic Cliff Lake plutonic complex.

Thrust-imbricates with a similar orientation can be inferred from aligned drillhole markers at higher structural levels in the Hook Lake block where clastic metasedimentary rocks (unit W) are in footwall contact with volcanic basement (SL4, Fig. 20). Intervals of tonalite exceeding thicknesses of 500 m. occur in the footwall and hanging wall of this structure, suggesting that the synvolcanic Cliff Lake pluton may also have been structurally repeated (Fig. 20).

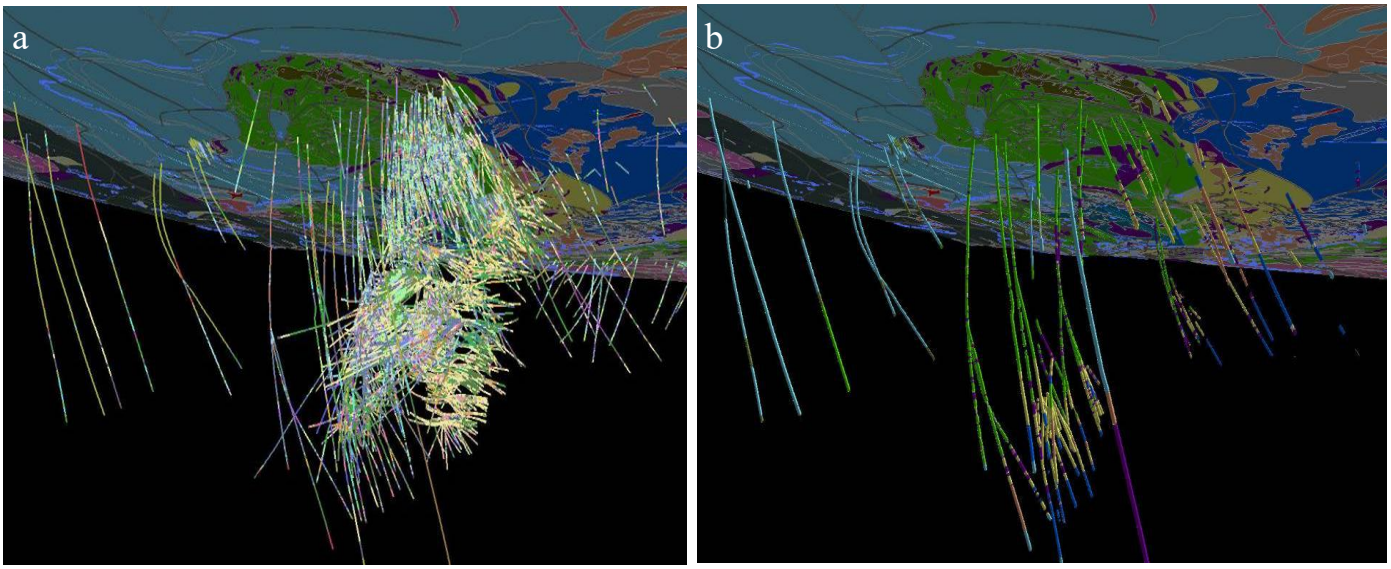

Figure 17 Lithostratigraphic encoding of industry drillholes used to build the camp-scale Flin Flon 3D model a) bedrock geological map and industry drillhole lithology logs; b) harmonized bedrock geological map and lithostratigraphic logs (after Schetselaar et al. 2016).

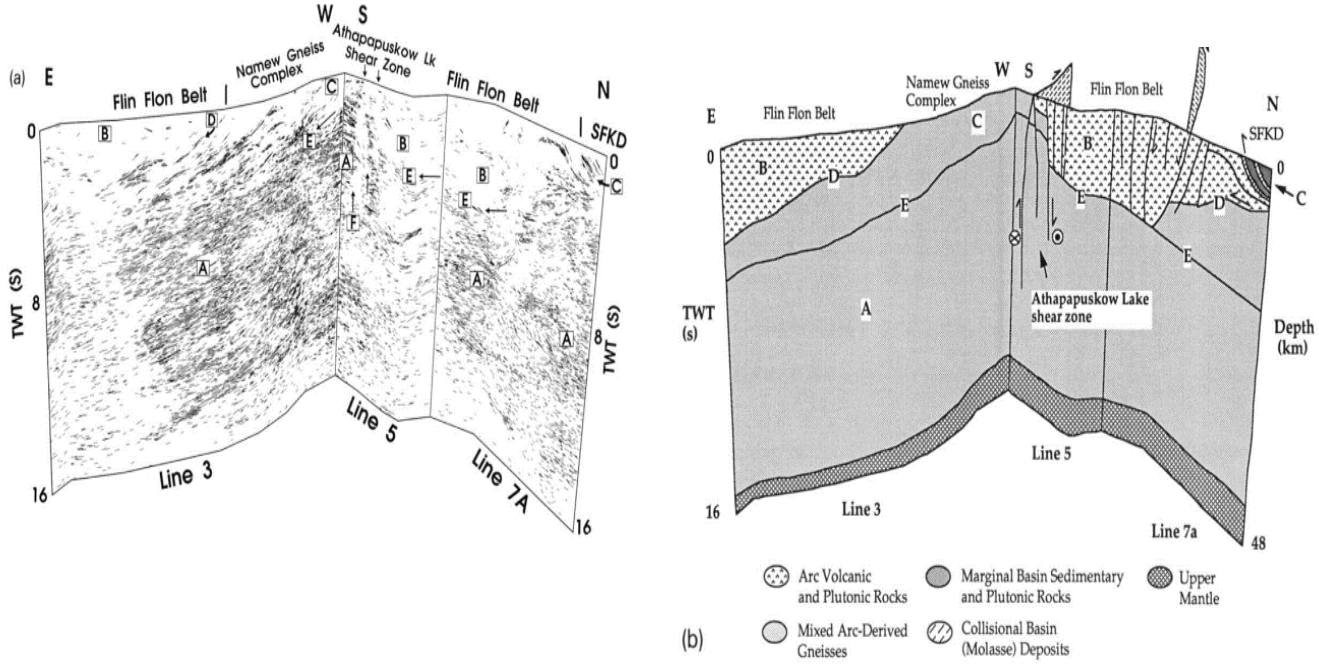

Figure 18 LITHOPROBE lines 3 and 7A and their interpretations (Lucas et al. 1994) to show typical level of detail of units and geological structures from LITHOPROBE seismic data. Note local differentiation of FFGC lithostratigraphic assemblages into Missi Group metasedimentary rocks (M) juvenile arc volcanic rocks and successor arc plutonic rocks (J & P) of the Flin Flon arc assemblage.

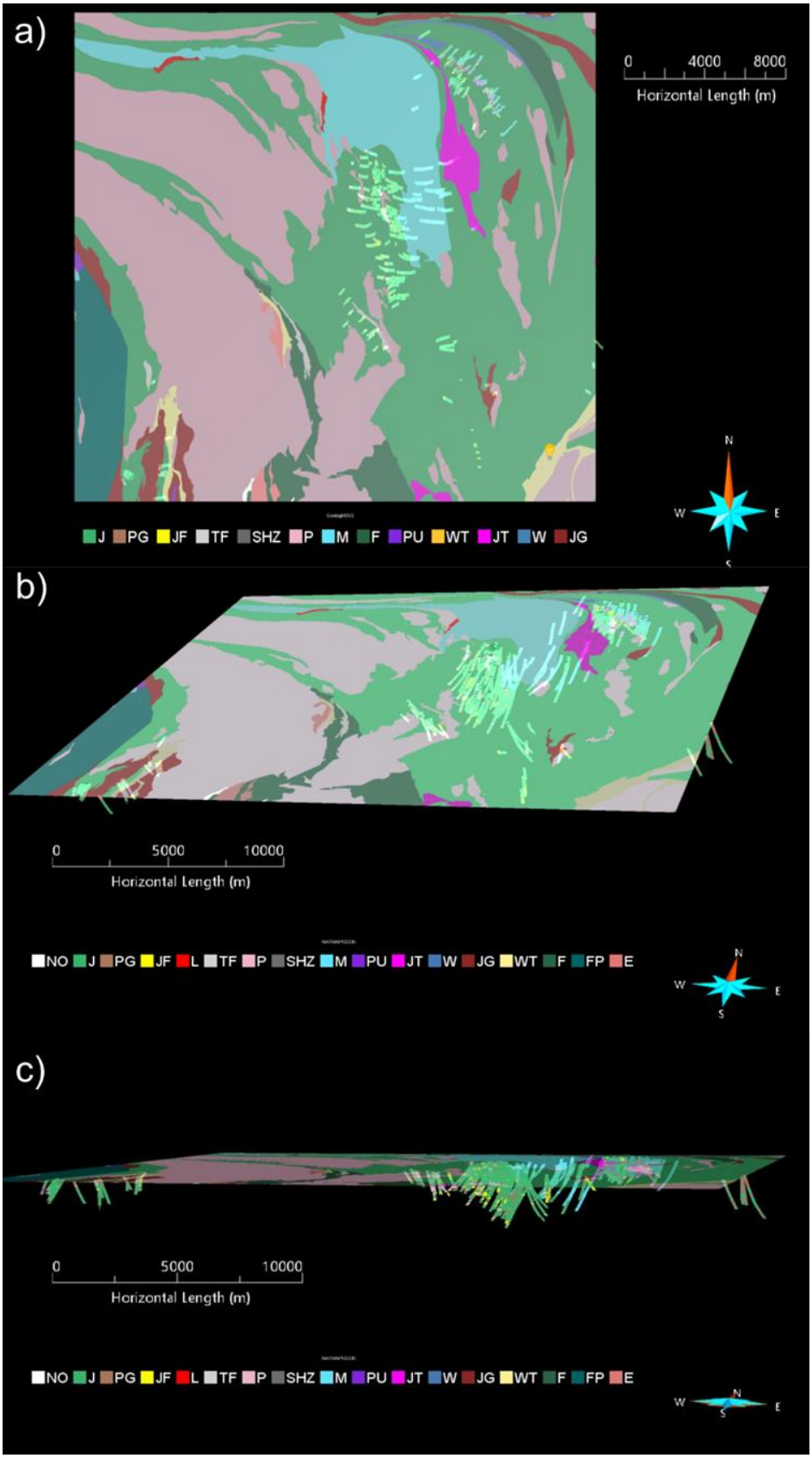

Figure 19 3D perspective views of the harmonized drillhole-bedrock compilation, including a) top view; b) oblique view from the southeast and c) frontal view from the south. See Table 3 for an explanation of geological unit codes.

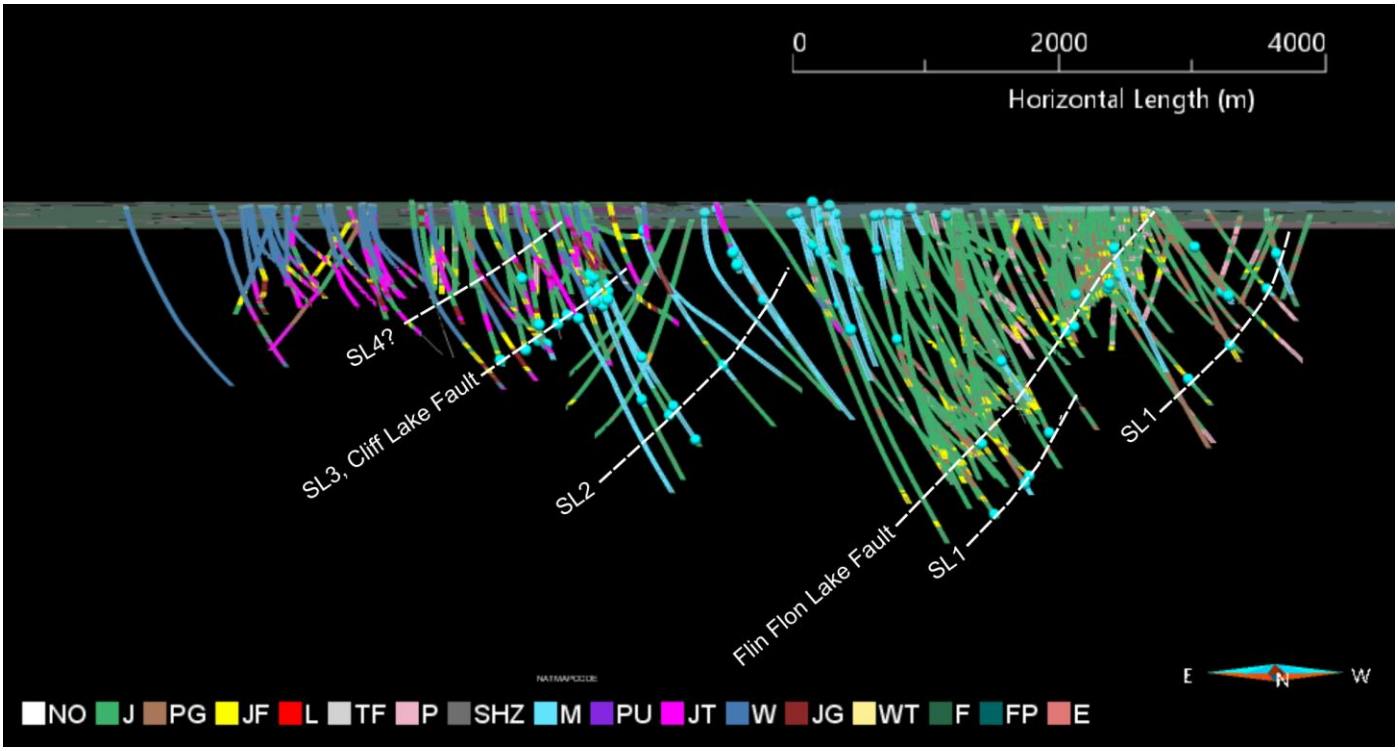

Figure 20 3D perspective view of harmonized drillhole-bedrock compilation to highlight regional scale west-vergent thrust imbrication. Blue balls indicate tops of Missi Group drillhole intervals. Stippled white lines trace alignment of these markers along major thrust faults (SL1–SL4). See Table 3 for an explanation of geological unit codes.

Cliff Lake fault

Missi Group metasedimentary rocks in the footwall of juvenile arc assemblage unit (J) and Cliff Lake pluton synvolcanic rocks (JT) constrain, together with its surface trace, the geometry and orientation of the Cliff Lake fault over a strike length of about 10 km (Figs. 16 and 21). The modelled fault structure dips between 15–45º and strikes between 320–20º (10–90 percentile ranges, Fig. 21b). Drillhole intervals of the Missi Group are consistently in footwall contact with volcanic basement rocks (units J and JT, Fig 21a) suggesting a significant component of post-Missi thrust faulting (D3, Lafrance et al. 2016). The displacement of metamorphic isograds along the Cliff Lake fault further towards the south is consistent with this interpretation (Lazzarotto et al. 2019). Structural mapping along its trace between the Hook Lake block and Flin Flon arc assemblages reported C/S fabrics with a sinistral sense of shear that were overprinted by tension gashes with a dextral component of shear (Kremer and Simard, 2007). These observations suggest that the Cliff Lake fault was repeatedly reactivated during the later transpressional (D5–D6) and post-metamorphic faulting (D7) phases of the deformation history (Lafrance et al. 2016).

Seismic reflections LITHOPROBE line 5

Considering the resolution and scale of the LITHOPROBE seismic lines, it can be challenging to attribute seismic reflections to their corresponding geological contacts and structures mapped at surface. The harmonized drillhole-bedrock compilation, extending in depth to about 2 km, can be used to overcome these challenges, at least in areas with a relatively high-density of drillholes. Figure 22 shows the drillhole-bedrock compilation with a section of LITHOPROBE line 5. In general, the seismic reflections are consistent in dip with the overall subsurface structure

highlighted by the regional alignment of drillhole unit contacts. Moreover, a previously modelled intra-Missi thrust imbricate of volcanic basement (Schetselaar et al. 2016; SL2 on Fig. 20) appears to correspond to a bundle of high-amplitude reflections on LITHOPROBE line 5, which can be traced to a depth of at least 8 km (Fig. 22). This interpretation will in turn constrain the regional geometry of the Missi Group thrust imbricate and Hook Lake block in the hanging wall of the Cliff Lake fault.

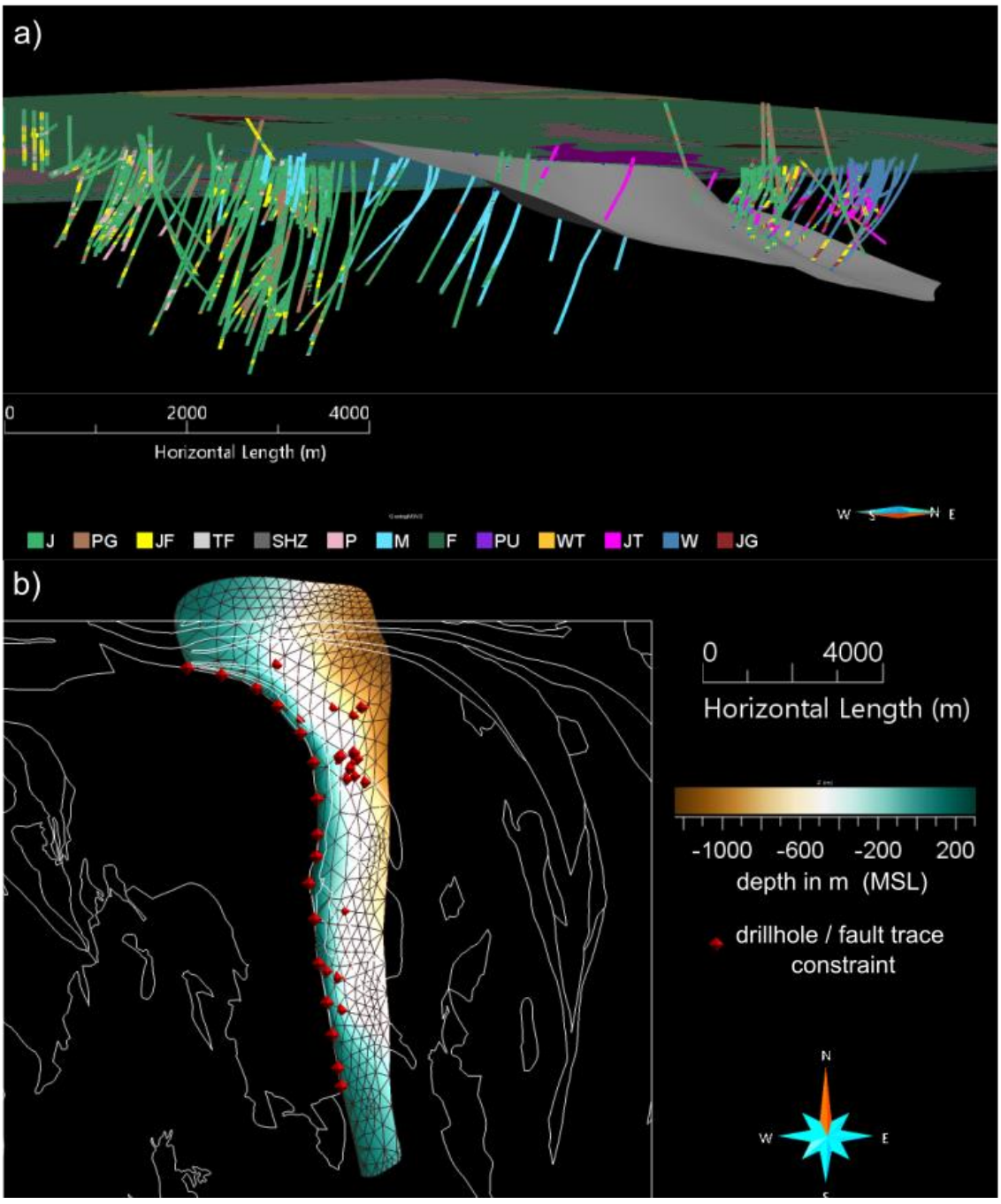

Figure 21 3D model of the Cliff Lake fault, a) oblique view with harmonized drillhole-bedrock compilation; b) Top view showing wireframe representation coloured with depth. White lines represent geological unit contacts from the generalized NATMAP bedrock map compilation.

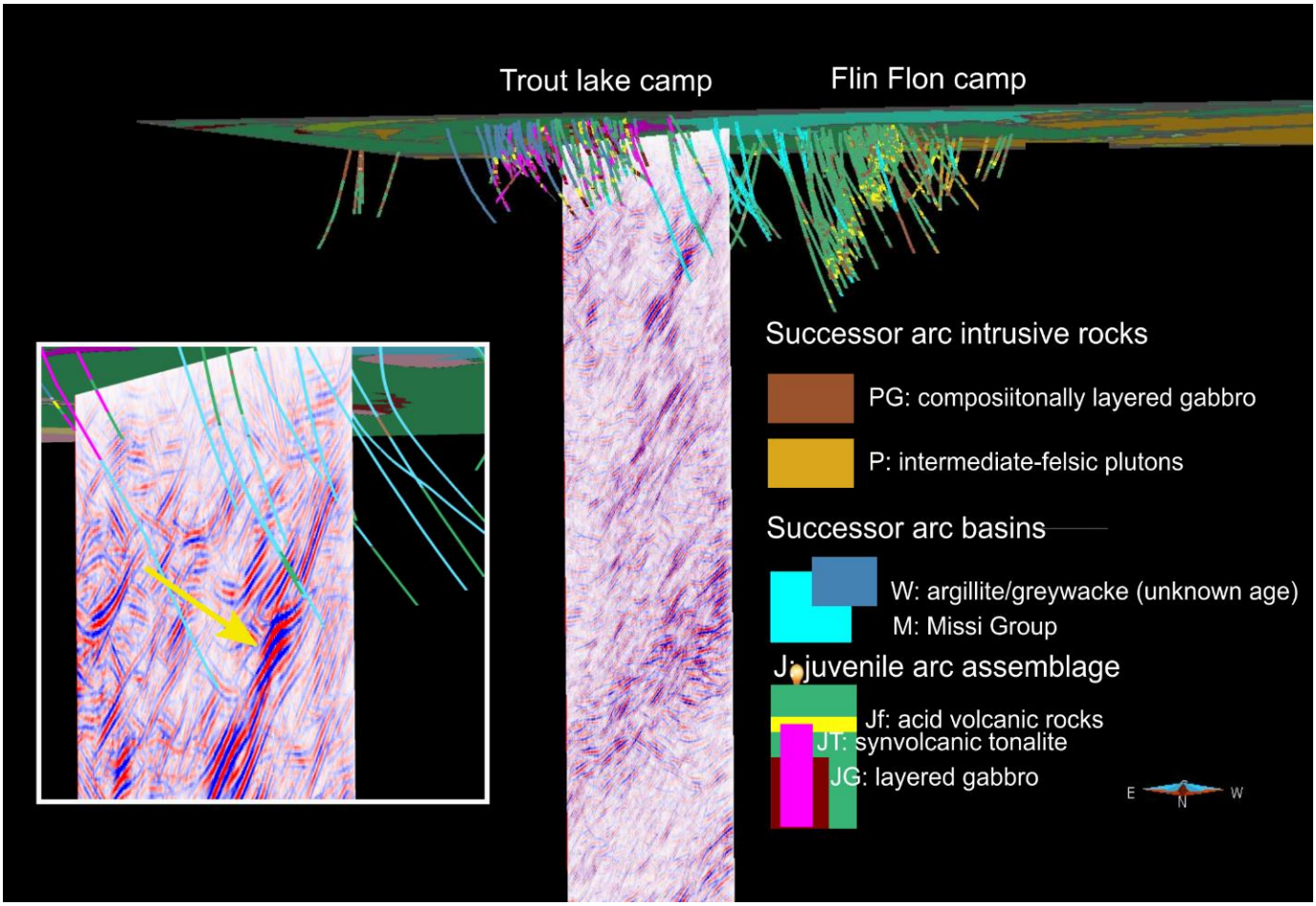

Figure 22 3D perspective view of the harmonized drillhole-bedrock compilation with segment of LITHOPROBE line 5. Yellow arrow in inset shows inference of the top of the intra-Missi Group thrust imbricate of mafic volcanic and volcaniclastic rocks (unit J). Note consistency between the apparent dip of the seismic reflections and aligned drillhole intervals.

Relevance to mineral exploration

Unravelling the regional subsurface structure of the FFGC will be instrumental for focusing exploration at larger distances from the numerous VMS mine camps. The harmonized drillhole-bedrock compilation in the test area, shows, in addition the earlier-described regional thrust imbrication, repeats of felsic volcanic units that may guide drill targeting and prevent the premature closure of drilling operations. These repeats include stacked intervals of the Millrock member hosting the massive sulfide ore lenses of the Triple 7 and Callinan deposits. Similar repeats of felsic intervals are apparent in the hanging wall of the Cliff Lake fault (Fig. 21a). Follow-up drill core logging of these felsic volcanic intervals may shed light on whether these repeats are stratigraphic or tectonic in origin, further guiding deep exploration. Insights into structural complexities, such as out-of-sequence or blind thrust imbricates may, in combination with geophysical surveys, drill core logging and more detailed 3D representation of drill lithology logs, benefit from the harmonized drillhole-bedrock compilation and provide spatial context in vectoring towards alteration and ore zones. The compilation may also provide a basis for more quantitative modelling approaches in which derived 3D geological models are input to forward (seismic) and inverse (MT, potential field) modelling routines.

PRELIMINARY CRUSTAL MODEL OF THE WESTERN FLIN FLON – GLENNIE COMPLEX

The objective of this sub-project was to build a preliminary 3D crustal model (Version 1.0) for the 200 x 300 km project area based on the existing LITHOPROBE Trans-Hudson Orogen Transect seismic data. The initial 3D model will provide a framework for constrained inversion of potential field and MT data and will eventually host the more detailed 3D models developed for the mining camps in the area. The original LITHOPROBE seismic interpretations (e.g., Lucas et al., 1994; Lewry et al., 1994; Hajnal et al., 1995; White et al., 1999) provide the basis for building this initial framework model. The model will subsequently be refined as re-analysis of the original data is conducted and as other data sets are integrated.

The workflow to construct the Version 1.0 model consisted of the following:

1. Seismic data were converted from time-to-depth using an average crustal velocity of 6000 m/s, and then imported to GOCAD using a smoothed version of the original acquisition line to register the profile locations. Figure 23 shows the network of seismic lines used.

2. Interpretation images from the original publications were imported and draped onto the seismic depth sections (Fig. 24).

3. Horizons corresponding to the major crustal tectonostratigraphic units and major faults were picked. For example, the Tabbernor and Sturgeon-Weir faults are shown in Figure 24 along with the picks of the Moho horizon. Tectono-stratigraphic horizons that were picked from the seismic data comprise top of Moho, Archean, arc-derived gneiss, arc-volcanics, and marginal basin rocks.

4. For each of the picked horizons, the corresponding points were used to construct a 3D surface. Figure 25-Left depicts the resultant surfaces for the Moho, top Archean and top of arc-derived gneiss. The Tabbernor and Sturgeon-Weir faults cut the upper surfaces, and a surface window of Archean rocks is observed. Figure 25-Right also includes the arc volcanics and marginal basin surfaces.

5. This 3D layered model was used to construct a solid 3D model as shown in Figure 26.

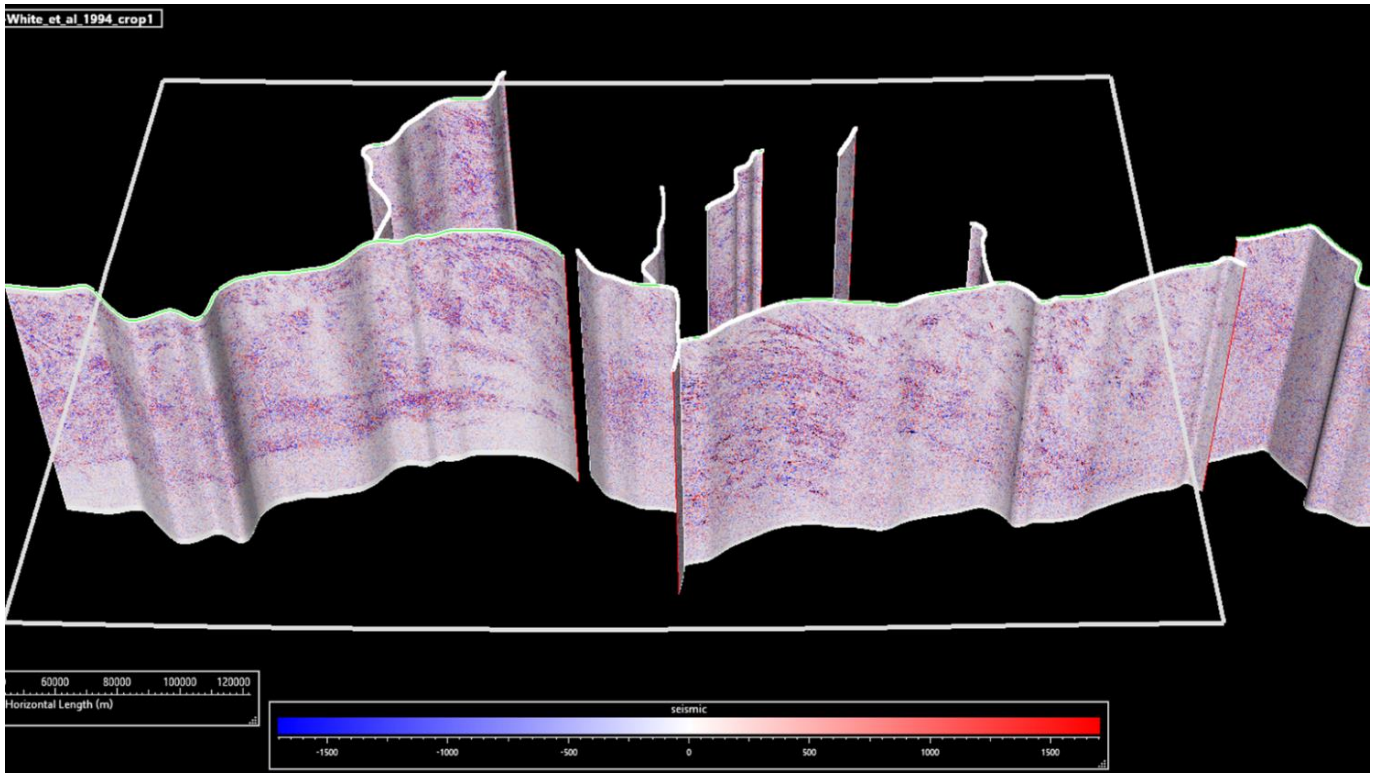

Figure 23 Network of seismic profiles that form basis for 3D crustal model (V 1.0). The project area is denoted by the white frame. The depth extent of the seismic sections is 54 km.

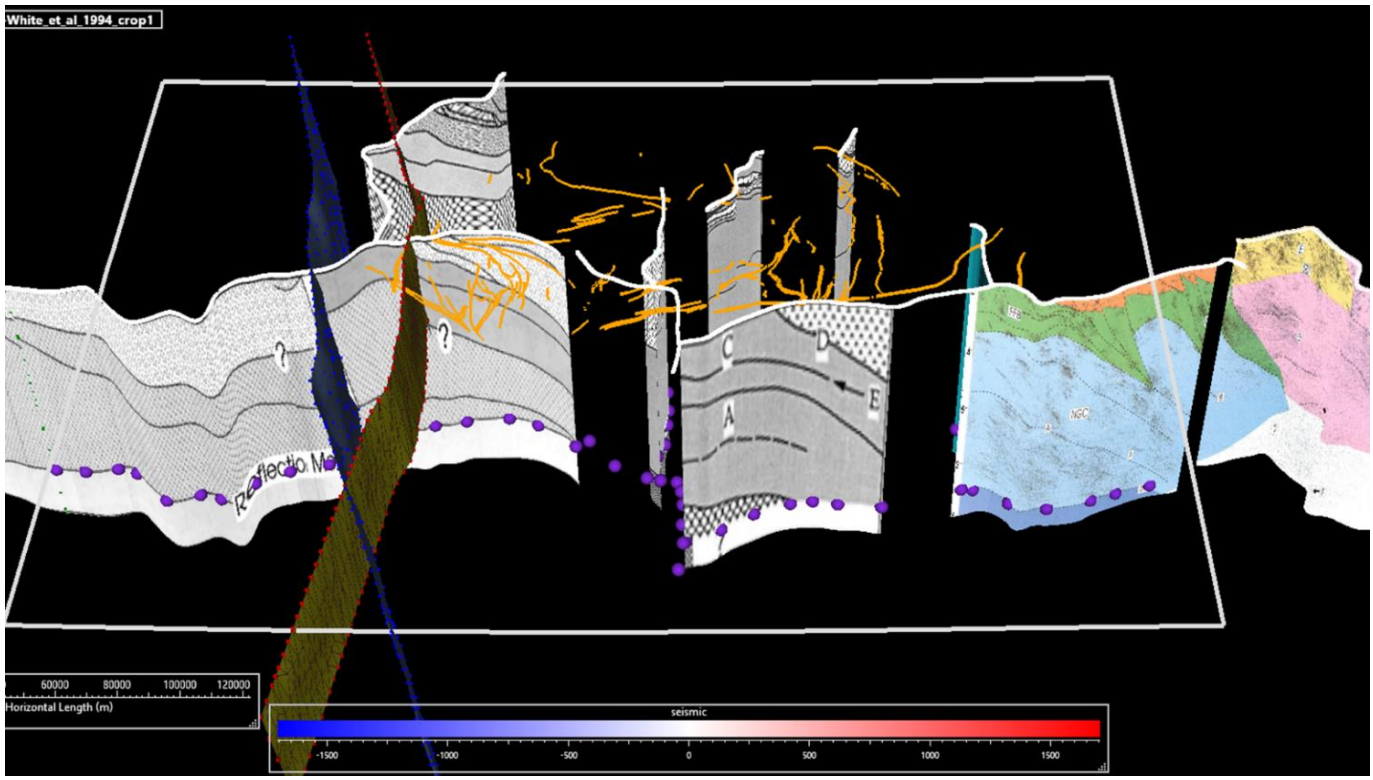

Figure 24 Original LITHOPROBE seismic interpretations draped onto the seismic surfaces. Also shown are selected shear zone surface traces (orange lines), steep-angle faults surfaces, and Moho horizon picks (purple spheres).

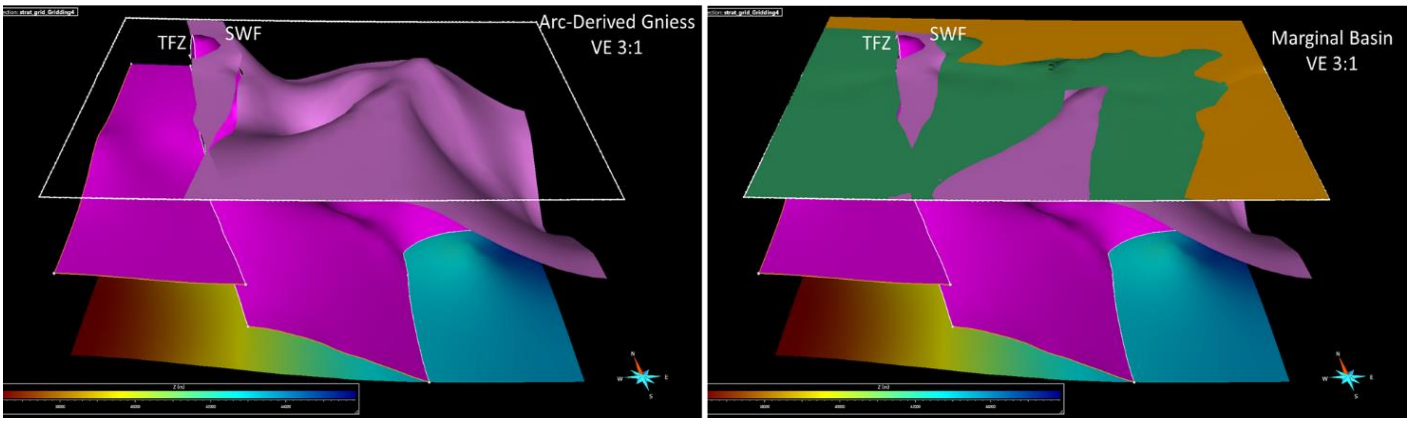

Figure 25 3D surfaces constructed from the seismic interpretations. Left: Shown are (from bottom to top) the Moho, Archean (Sask craton) and arc-derived gneiss. Also shown are the Tabbernor (TFZ) and Sturgeon-Weir (SWF) faults. Vertical exaggeration is 3:1. Right: uppermost horizons are arc-derived volcanic and marginal basin rocks.

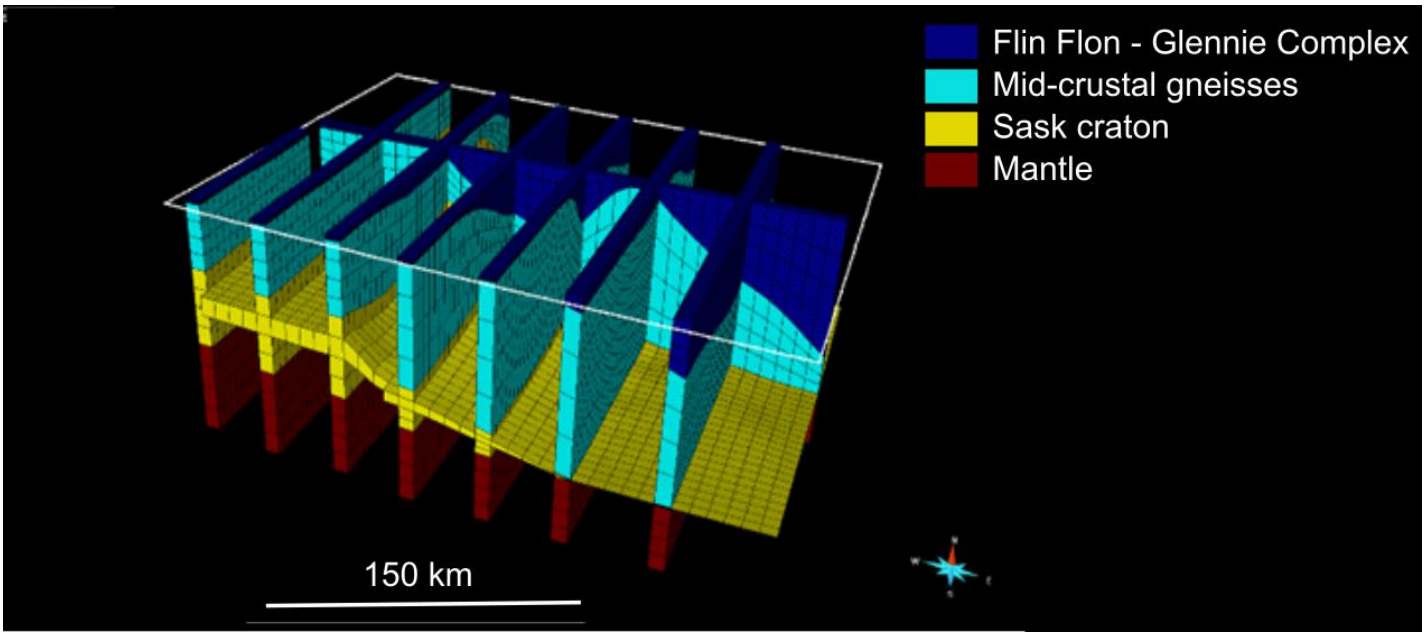

Figure 26 3D crustal-scale solid model.

ACKNOWLEDGEMENTS

Hudbay Minerals Inc. is acknowledged for sharing their drillhole and geophysical exploration data. The preliminary interpretations benefitted from discussions with Ralf Maxeiner and Kyle Reid of respectively the Saskatchewan and Manitoba geological surveys.

REFERENCES

Akaranta, O. 2011. Evaluation of the resistivity structure of the Flin Flon Belt and the Chisel Lake Area using the magnetotelluric method. B.Sc. thesis, University of Manitoba, 153 p.

Ansari, M., Schetselaar, E., Craven, J., Farquharson, C. 2020. Three-dimensional magnetotelluric numerical simulation of realistic geologic models. Geophysics,85(5), p. E171-E190, https:/doi.org/10.1190/geo2019-0214.1.

Boulanger, O. and Chouteau, M. 2001. Constraints in 3D gravity inversion. Geophysical Prospecting v. 49, p. 265-280, https:/doi.org/10.1046/j.1365-2478.2001.00254.x.

Corrigan, D., Pehrsson, S., Wodicka, N. and de Kemp, E. 2009. The Paleoproterozoic Trans-Hudson Orogen: a prototype of modern accretionary processes. Journal of the Geological Society of London, Special Volume "Ancient Orogens and Modern Analogues". In: Murphy, J. B., Keppie, J. D. and Hynes, A. J. (eds.) Ancient Orogens and Modern Analogues. Geological Society, London, Special Publications, v. 327, p. 457-479, https:/doi.org/10.1144/SP327.19.

De Kemp, E.A., Schetselaar, E.M., Hillier, M.J., Lydon, J.W., Ransom, P.W. 2017. Assessing the workflow for regional-scale 3D geologic modeling: An example from the Sullivan time horizon, Purcell Anticlinorium East Kootenay region, southeastern British Columbia. Interpretation 4, p. 33-50, https://doi.org/10.1190/INT-2015-0191.1.

Ferguson, I. J., Stevens, K.M., Jones, A.G., 2005. Electrical-Resistivity Imaging of the Central Trans-Hudson Orogen. Canadian Journal of Earth Sciences v. 42, p. 495-515, https:/doi.org/10.1139/e05-017.

Galley, A. G., Syme, E.C. and Bailes, A.H. 2007. Metallogeny of the Paleoproterozoic Flin Flon Belt, Manitoba and Sakatchewan *in* Goodfellow, W.D. ed., Mineral deposits of Canada: A synthesis of major deposit types, district metallogeny, the evolution of geological provinces and exploration methods: Geological Association of Canada, Mineral Deposit Division, Special Publication No. 5, p. 509-531.

Gibson, H.L., Allen, R.L., Riverin, G. and Lane, T.E. 2007. The VMS model: advances and application to exploration targeting. In "Proceedings of Exploration 07: Fifth Decennial International Conference on Mineral Exploration" edited by B. Milkereit, 2007, p. 713-730.

Hajnal, Z., Lucas, S.B., White, D.J., Lewry, J., Bezdan, S., Stauffer, M.R. and Thomas, M.D. 1995. Seismic reflection images of strike-slip faults and linked detachments in the Trans-Hudson Orogen, Tectonics, v. 15, p. 427-439, https:/doi.org/10.1029/95TC02710.

Jones, A. G., Ledo, J., Ferguson, I. J. 2005. Electromagnetic Images of the Trans-Hudson Orogen: The North American Central Plains Anomaly Revealed. Canadian Journal of Earth Sciences v. 42, p. 457–78, https:/doi.org/10.1139/e05-018.

Kelbert, A., Meqbel, N., Gary D. Egbert, G.D., and Tandon, K., 2014. ModEM: A Modular System for Inversion of Electromagnetic Geophysical Data. Computers and Geosciences v. 66, p. 40–53, https:/doi.org/10.1016/j.cageo.2014.01.010.

Kremer, P.D. and Simard, R-L. 2007. Geology of the Hook Lake Block, Flin Flon area, Manitoba (part of NTS 63K12); *in* Report of Activities 2007, Manitoba Science, Technology, Energy and Mines, Manitoba Geological Survey, p. 21-32, https://www.manitoba.ca/iem/geo/field/roa07pdfs/GS-2.pdf.

Lafrance, B., Gibson, H.L., DeWolfe, M., Pehrsson, S., Schetselaar, E., DeWolfe, Y.M., Lewis, D. 2016, Structural reconstruction of the Flin Flon volcanogenic massive sulfide mining district, Saskatchewan and Manitoba, Canada. Economic Geology, v. 111, p. 849-875, https:/doi.org/10.2113/econgeo.111.4.849.

Lazzarotto, M., Pattison, D.R.M., Gagné, S., Starr, P.G. 2020, Metamorphic and structural evolution of the FP.G. on-Athapapuskow Lake area, west-central Manitoba. Canadian Journal of Earth Sciences, v. 57, p. 1269-1288, https:/doi.org/10.1139/cjes-2019-0136.

Leclair, A.D., Lucas, S.B., Broome, H.J., Viljoen, D.W. and Weber, W. 1997: Regional mapping of Precambrian basement beneath Phanerozoic cover in southeastern Trans-Hudson Orogen, Manitoba and Saskatchewan; Canadian Journal of Earth Sciences, v. 34, p. 618–634, https:/doi.org/10.1139/e17-049.

Lewry, J.F., Z. Hajnal, Z., Green, A., Lucas, S.B., White, D., Stauffer, M.R., Ashton, K.E., Weber, W. and Clowes, R. 1994. Structure of a Paleoproterozoic continent-continent collision zone: A Lithoprobe seismic reflection profile across the Trans-Hudson Orogen, Canada, Tectonophysics, v. 232, p. 143-160, https://doi.org/10.1016/0040-1951(94)90081-7.

Lucas, S., Green, A., Hajnal, Z., White, D., Lewryp, J. Ashton K., Weber, W. and Clowes R. 1993. Deep seismic profile across a Proterozoic collision zone: surprises at depth. Nature 363, p. 339–342, https://doi.org/10.1038/363339a0.

Lucas, S. et al., 1994. Three-dimensional collisional structure of the Trans-Hudson Orogen, Canada. Tectonophysics, v. 232, p. 161-178, https://doi.org/10.1016/0040-1951(94)90082-5.

Lucas, S.B., Stern, R.A., Reilly, B.A., Thomas, D.J. 1996. Intraoceanic tectonics and the development of continental crust; 1.92-1.84 Ga evolution of the Flin Flon belt, Canada, Bulletin of the Geological Association of America, v. 108, p. 602-629, https://doi.org/10.1130/0016-7606(1996)108<0602:ITATDO>2.3.CO;2.

Lucas, S.B., Syme, E.C. and Ashton, K.E., 1999. New perspectives on the Flin Flon Belt, Trans-Hudson Orogen, Manitoba and Saskatchewan: an introduction to the special issue on the NATMAP Shield Margin Project, Part 1., Canadian Journal of Earth Sciences, v. 36, p. 135-140, https:/doi.org/10.1139/e99-055.

Morelli, R.M. 2012. Regional data compilation and three-dimensional geological modelling in the vicinity of the Shield margin, Hanson Lake area *in* Summary of Investigations 2012, Volume 2, Saskatchewan Geological Survey, Sask. Ministry of the Economy, Misc. Rep. 2012-4.2, Paper A-8, 12 p.

NATMAP Shield Margin Project Working Group, 1998, "Geology, NATMAP Shield Margin Project area, Flin Flon Belt, Manitoba/Saskatchewan", Geological Survey of Canada, "A" Series Map 1968A, 1998, 54 pages (9 sheets) https://doi.org/10.4095/210073.

Pilkington, M., 2009. 3D magnetic data-space inversion with sparseness constraints, Geophysics, v. 74, p. L7–L15, https://doi.org/10.1190/1.3026538

Schetselaar, E., Pehrsson, S., Devine, C., Lafrance, B., White D., Malinowski, M. 2016. 3D geologic modeling in the Flin Flon Mining district, Trans-Hudson orogen, Canada: Evidence for polyphase imbrication of the Flin Flon-777-Callinan volcanogenic massive sulfide ore system. Economic Geology v. 111, p.877–901, https://doi.org/10.2113/econgeo.111.4.877.

Schetselaar, E., Bellefleur, G., Craven, J., Roots, E., Cheraghi, S., Shamsipour, P., Caté, A., Mercier-Langevin, P., El Goumi, N., Enkin, R., Salisbury, M. 2018 Geologically driven 3D modelling of physical rock properties in support of interpreting the seismic response of the Lalor volcanogenic massive sulphide deposit, Snow Lake, Manitoba, Canada. Geological Society London Special Publications v. 45, p. 57-79, https://doi.org/10.1144/SP453.5.

Simard, R-L. and McGregor, C.R. 2009: Toward a new sub-Phanerozoic Precambrian basement map of the Flin Flon Belt, Manitoba (parts of NTS 63J, K, L); in Report of Activities 2009, Manitoba Innovation, Energy and Mines, Manitoba Geological Survey, p. 15–21, https://www.manitoba.ca/iem/geo/field/roa09pdfs/GS-2.pdf.

Simard R-L., MacLachlan K., Gibson H.L., DeWolfe Y.M., Devine C., Kremer, P.D., Lafrance B., Ames D.E., Syme E.C., Bailes A.H., Bailey K., Price D., Pehrsson S., Cole E., Lewis D. and Galley A.G. 2010. Geology of the Flin Flon area, Manitoba and Saskatchewan (part of NTS 63K12, 13); Manitoba Innovation, Energy and Mines, Manitoba Geological Survey, Geoscientific Map MAP2010-1 and Saskatchewan Ministry of Energy and Resources, Geoscience Map 2010-2, 1 colour map, scale 1:10,000.

St-Charles, P.-L., Rousseau, B., Ghosn, J., Nantel, J.P., Bellefleur, G., and Schetselaar, E., 2021. A multi-survey dataset and benchmark for first break picking in hard rock seismic exploration. Expended abstract presented at the workshop on Machine Learning and the Physical Sciences held as part of the 35th Neurips conference, Vancouver, December 2021. https://ml4physicalsciences.github.io/2021/files/NeurIPS_ML4PS_2021_3.pdf

Stern, R.A., Syme, E.C. and Lucas, S.B. 1995. Geochemistry of 1.9 Ga MORB- and OIB-like basalts from the Amisk collage, Flin Flon belt, Canada: evidence for an intra-oceanic origin. Geochimica et Cosmochimica acta, v. 59, p. 3131-3154, https://doi.org/10.1016/0016-7037(95)00202-B.

Stern, R.A., Machado, N., Syme, E.C., Lucas, S.B., David, J. 2000. Chronology of crustal growth and recycling in the Paleoproterozoic Amisk collage (Flin Flon Belt), Trans-Hudson Orogen, Canada. Canadian Journal of Earth Sciences, v. 36, p. 1807-1827, https://doi.org/10.1139/e99-028.

Syme, E.C., Lucas, S.B., Bailes, A.H., Stern, R.A. 1999. Contrasting arc and MORB-like assemblages in the Paleoproterozoic Flin Flon Belt, Manitoba, and the role of intra-arc extension in localizing volcanic-hosted massive sulphide deposits. Canadian Journal of Earth Sciences v. 36, p. 1767-1788, https://doi.org/10.1139/e98-084.

Ugalde, H., 2019, Aeromagnetic data compilation – Flin Flon and Snow Lake ares, Manitoba. Unpublished report submitted to Hudson Minerals by Dip Geosciences.

White, D.J., Jones, A.G., Lucas, S.B., and Hajnal, Z., 1999. Tectonic evolution of the Superior Boundary Zone from coincident seismic reflection and magnetotelluric profiles, Tectonics, v. 18, p. 430-451, https://doi.org/10.1029/1999TC900002.